Low energy electrodynamics of high Tc superconductors

Feenstra, Bokke Johannes

Publication date:
1997

Link to publication in University of Groningen/UMCG research database

Citation for published version (APA):
Feenstra, B. J. (1997). *Low energy electrodynamics of high Tc superconductors*. s.n.

Chapter 7

Nonequilibrium Superconductivity studied by Photo Induced Activation of Mm-Wave Absorption (PIAMA)

7.1 Introduction

For both the fundamental aspects and for applications, a proper understanding of the dynamical behavior of quasiparticles in the high T_c cuprates is essential. Fundamentally, the behavior of the quasiparticle scattering rate, τ, as a function of frequency and temperature yields important information on the interior of the HTSC's. In the normal state, the linear dependencies of $1/\tau$ on T and ω are indicative of a breakdown of the Landau Fermi liquid formulation applicable to normal metals [1]. The linear dc-resistivity, which extrapolates to $\rho = 0$ for $T = 0$, leads to the very surprising conclusion that phonon scattering is insignificant over a large range of several hundreds of Kelvins. Moreover, since the Fermi liquid theory is one of the basic ingredients of the BCS-theory, these experimental observations have posed an important question as to which approach one should use in attempting to explain the superconductivity in the cuprates [2].

In the superconducting state, the quasiparticle scattering rate also yields important information. Most importantly, a strong enhancement of τ has been observed just below T_c [3,4]. This observation provides additional evidence that the scattering has an electronic rather than a phononic origin. Much of the contemporary data on τ have been acquired indirectly, for instance by assuming that the two-fluid description is valid for these materials [5,6]. A direct measurement of the decay processes is therefore desirable.

For applications, the presence of quasiparticles and their dynamics are of crucial importance, since a large number of low-energy excitations will inevitably lead to undesired losses. Furthermore, high T_c films are considered to have considerable potential as FIR-detectors [7]. In order to make optimal use of such detectors one needs to disentangle the bolometric and non-bolometric contributions, since the latter is thought to give rise to very fast response times [8].

In the seventies, similar motivations to distinguish the bolometric and non-bolometric contributions lead to a widespread interest in experiments exploring non-equilibrium superconductivity. Both experimentally and theoretically, people have been trying to answer questions such as the influence of the excess energy given to quasiparticles in the pair-breaking process [9,10] and the processes determining the quasiparticle lifetime [11–13]. A more detailed overview of the research concerning these topics has been given in section 2.3.

In all the above considerations the symmetry of the order parameter will be an essential ingredient. Not only will it have a large influence on the quasiparticle density, but it will also greatly affect their dynamics. Obviously, when the superconductor has an isotropic gap a certain minimum energy is needed to create quasiparticles. Therefore, at sufficiently low temperatures, the thermally excited quasiparticle density will be negligible. However, the presence of nodes opens up a channel in which quasiparticles can be created at infinitesimally small energies. As a result the quasiparticle density has a power law dependence on temperature, as opposed to the exponential dependence for the case of an s-wave gap. Moreover, one can imagine that having an anisotropic energy gap will modify the decay channels for excited quasiparticles, thereby altering their relaxation rate.

In this chapter we present a new method to study the quasiparticle dynamics: Photo Induced Activation of Mm-wave Absorption (PIAMA). With this technique we use two independent sources in a pump-probe configuration. The first creates a temporary excited state within the superconducting thin film, while the second monitors the time evolution of the state. A more detailed description of the experimental setup can be found in chapter 4. As the pump, we used the free electron laser, FELIX, located at the user facility of the FOM-institute "Rijnhuizen" in Nieuwegein, The Netherlands [14]. FELIX is tunable over a wide frequency range (100 - 2000 cm^{-1}), reaching energies comparable to the relevant energy scales in HTSC's, such as phonon energies and the superconducting energy gap. PIAMA resembles earlier photoconductivity [15,16] and pump-probe experiments [17,18], although there are some essential differences. First of all, the frequencies of the pump and probe differ by approximately two orders of magnitude, in contrast to most pump-probe experiments where they have the same frequency. Secondly, we measure the system response at ac-frequencies (5 cm^{-1}) instead of using the dc-response, as is done in photoconductivity experiments. This facilitates measurements in the superconducting state since the *ac*-resistivity of a superconductor is nonzero. Furthermore, the pump frequency is tunable and has a relatively low energy, within the FIR and MIR region, whereas in most other experiments a single frequency visible laser was used. This allows us to study PIAMA both as a function of frequency and temperature.

First we will present the scope of the experiment, explaining in detail what happens to a superconductor when it is illuminated by an FIR-pulse. In particular, the relevant time scales and decay processes will be treated, with attention to the question of the symmetry of the order parameter. In the next section, results on a conventional superconductor, NbN, will be presented, while in section 7.4 the results of the PIAMA experiments on one of the cuprates, $DyBa_2Cu_3O_{7-\delta}$, will be discussed. In both cases attention will be paid to disentangling equilibrium and non-equilibrium contributions. Furthermore, in section

7.4 the correlation between the quasiparticle dynamics and the pairing symmetry will be discussed, demonstrating the drastic consequences of a d-wave symmetry on the recombination process.

7.2   Scope of the Experiment

What Happens during an FIR-pulse?

First we need to visualize what will happen to a superconductor when it is subjected to a pulse of far-infrared radiation. The FIR-radiation will change the initial state of the superconductor by changing the balance between the number of Cooper pairs, n_{CP}, and the number of quasiparticles, n_{qp}. In fig. 7.1 we have sketched the effective electron temperature, T^*, and the quasiparticle density, n_{qp}. Indicated are several processes which are occurring, each having their own specific time scales:

A - build up

B - cascade

C - thermalization

D - recombination

E - bolometric response

During the FIR-pulse, the build up (A) of a temporary excited state occurs, having a response time of about 1 ps. During this process, both the electron temperature and the number of quasiparticles are enhanced. After the termination of the pulse, indicated by the first vertical dashed line in fig. 7.1, a cascading process (B) reduces the average energy of the electrons, thereby lowering T^*. During the cascade, quasiparticles having sufficient kinetic energy, break up additional Cooper pairs. Therefore, even though T^* decreases, n_{qp} increases even further. The time constant associated with the cascading process has been estimated to be approximately 1 ps or even faster [17]. On a longer time scale of about 1 ns [15] thermalization (C) via scattering processes lowers T^* even further, while now the quasiparticle density remains constant. In order to reduce also n_{qp} to its initial value, quasiparticles will have to recombine to form Cooper pairs (D). The time scale involved in the recombination process is rather difficult to disentangle from other processes and will be discussed in detail for the case of $DyBa_2Cu_3O_{7-\delta}$ at the end of this chapter.

In addition to the electronic processes mentioned above, a simple heating of the sample can also be present (E). This bolometric effect will have a slow relaxation time within the μs to ms-range, which is closely connected to the experimental configuration, since the additional thermal energy of the sample has to be carried away via its environment.
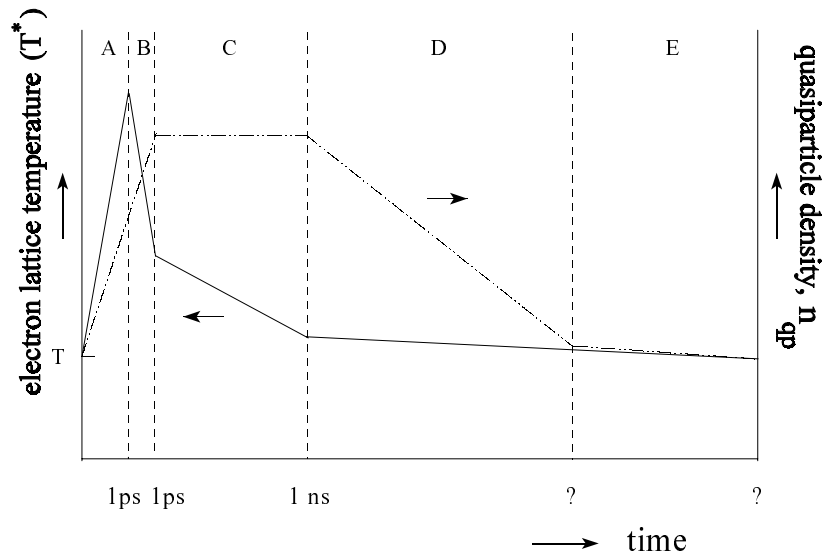
Figure 7.1: *Schematic representation of the effective electron temperature T^* (solid line), and the number of quasiparticles in a superconductor, n_{qp} (dash-dotted line), during and after being illuminated with an FIR-pulse.*
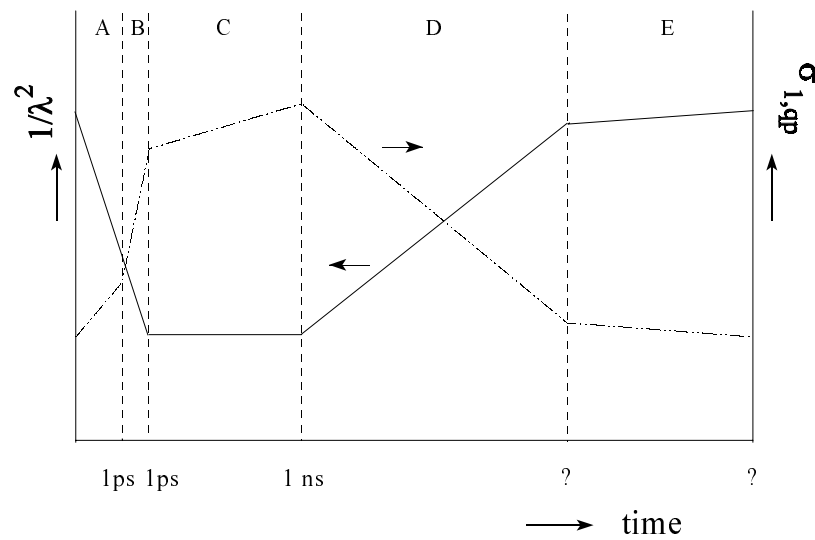

Figure 7.2: *Schematic representation of the optical response functions $1/\lambda^2$ (solid line) and $\sigma_{1,qp}$ (dash-dotted line) of a superconductor, during and after being illuminated with an FIR pulse.*

Optical Response Functions

The changes in quasiparticle and Cooper pair densities are reflected in the *complex* optical conductivity, which is, in the low temperature limit, given by:

$$\sigma_1 = \frac{e^2 \tau_{qp}}{m_{qp}} * n_{qp}$$

$$\sigma_2 = \frac{e^2}{\pi \nu m_e} * n_{CP} = \frac{c^2}{8\pi^2 \nu \lambda^2}$$

$$(7.1)$$

which is the physical quantity that determines the mm-wave transmission coefficient, Tr.

$$Tr = \frac{4p^2}{(1+p^2)^2 + (1+p^2)[\frac{4\pi d\sigma_1}{c}]^2 + (1+p^2)\frac{8\pi d\sigma_1}{c} + \frac{d^2 c^2}{\lambda^4 \omega^2}} \qquad (7.2)$$

where p is the complex refractive index of the substrate. We use the approximate transmission coefficient for the case of a minimum in the interference pattern of the bare substrate. From fig. 6.11 on page 105, it can be seen that for the 20 nm thick $DyBa_2Cu_3O_{7-\delta}$ film used during the PIAMA experiments, this is approximately valid at the probe frequency, 150 GHz. The time dependence of both σ_1 and $1/\lambda^2$ has been depicted in fig. 7.2. Since $1/\lambda^2 \sim n_{CP}$ and $2n_{CP} = n_{el,tot} - n_{qp}$, the changes in $1/\lambda^2$ during the subsequent processes A-E are simply opposite to the changes in n_{qp}, indicated in fig. 7.1.

However, as can be seen in equation (7.1), the change in the real part of the conductivity due to the quasiparticles, $\Delta\sigma_{1,qp}$, not only depends on the density, but also on the scattering rate, $\gamma_{qp} = 1/\tau_{qp}$. As mentioned above, the thermalization process connected to the modifications in the quasiparticle scattering rate, apart from the bolometric contribution, occur on a time scale of approximately 1 ns. This indicates that while $\Delta\sigma_{1,qp}$ is due to a combined effect of n_{qp} and τ_{qp} on this time scale, in our case, having a temporal resolution of about 1 μs, we will merely be sensitive to changes in σ_1 due to an altered n_{qp}.

Equilibrium vs. Non-equilibrium

We can divide the response of the optical conductivity to the presence of a short FIR-pulse into two specific cases:

- Equilibrium or bolometric

- Non-equilibrium or non-bolometric

The real part of the optical conductivity, σ_1 is plotted schematically in fig. 7.3 for both cases, where the left panel represents the initial state and the right panel represents the temporary state caused by the pulse. The pertinent parameters are given in table 7.1.

In all panels n_{qp} is represented by a Drude contribution having a width equal to γ_{qp}, while n_{CP} is represented by a δ-function, indicated here as the arrow at zero frequency. The strength of the δ-function is equivalent to the Cooper pair density, and therefore also

Equilibrium

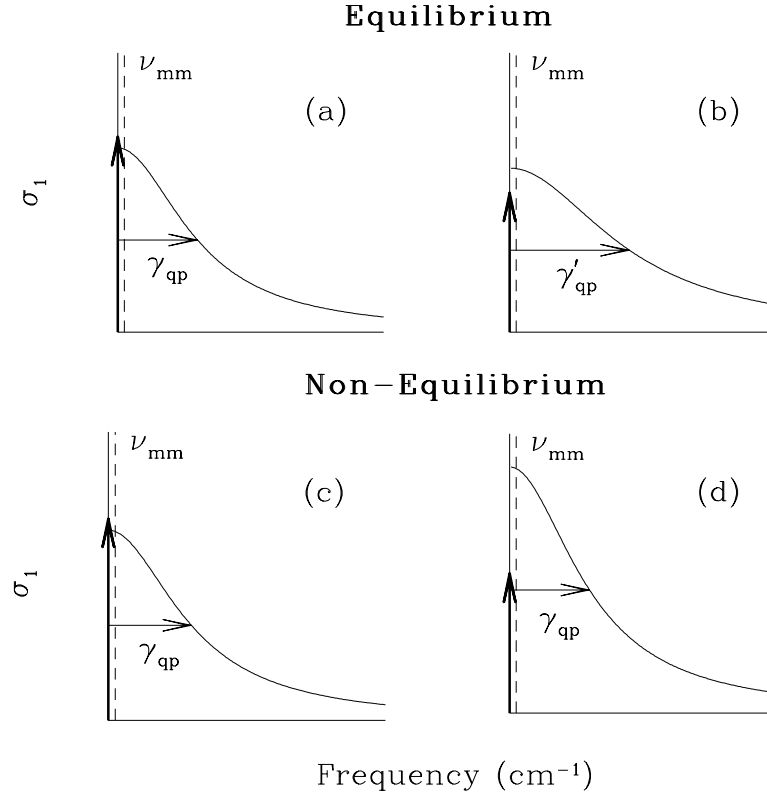**Non−Equilibrium**

Frequency (cm^{-1})

Figure 7.3: *Upper panels: change in optical conductivity, assuming an equilibrium response. a: initial state, b: superconductor at an elevated temperature. Lower panels: change in σ_1 in the non-equilibrium case. c: initial state, d: superconductor having a shifted chemical potential at the same temperature as the initial state.*

directly related to the magnitude of the dispersive part of the conductivity, σ_2, as was shown in eq. (7.1).

In the upper panel of fig. 7.3 we indicate what we choose to call the equilibrium process. In this scenario the absorbed radiation will temporarily raise the temperature of the entire sample, while the quasiparticle chemical potential, μ_{qp} remains in equilibrium with its environment. At the elevated temperature the number of Cooper pairs will be reduced and hence the penetration depth λ will be enhanced. Looking at the transmission given by eq. (7.2) we see that as a result, the last term in the denominator will be smaller and hence the transmission will increase. At the same time, the spectral weight removed from the superfluid δ-function will be transferred into the quasiparticle peak, thereby enhancing σ_1 and thus *reducing* the transmission coefficient. In addition to the transfer of spectral weight, the scattering rate γ_{qp} will also be enhanced, since the sample is now at an elevated temperature. This in turn tends to reduce σ_1 and thus enhance the transmissivity. The result will be a competition of all three phenomena mentioned above. In order to get

panel	ω_{pn} (cm^{-1})	γ_{qp} (cm^{-1})	ω_{ps} (cm^{-1})
a	7700	300	6400
b	8900	450	4600
c	7700	300	6400
d	8900	300	4600

Table 7.1: *Parameters used for the calculation of the real part of the conductivity, σ_1, presented in fig. 7.3.*

an idea of what might happen in this equilibrium case, it is very instructive to monitor the temperature dependence of the *unperturbed* transmission coefficient, since the process described above is not different from having a superconductor at a temporary elevated temperature. The results presented in chapter 6 show that at all frequencies the temperature dependence is monotonic. Therefore the equilibrium response will always show an enhanced transmissivity due to the presence of an FIR-pulse.

In the lower two panels we consider what we call the non-equilibrium response. In contrast to the equilibrium response, it is envisaged that the quasiparticle density is increased, while the actual sample temperature remains the same. Therefore, in this case the sample temperature is in equilibrium with its environment, while the quasiparticle chemical potential, μ_{qp}, is shifted. Just as in the equilibrium situation there are two competing contributions determining the value of the mm-wave transmissivity: on the one hand λ will be larger, or equivalently the screening of the superfluid will be reduced, enhancing the transmissivity. On the other hand the increased quasiparticle density will give rise to a larger σ_1, or equivalently a larger absorption, thereby *reducing* the transmission. Moreover, in contrast to the equilibrium response, the scattering rate γ_{qp} will be identical to the scattering rate in the initial state up to first order, justifying the conclusion that the enhanced absorption due to σ_1 will tend to reduce the mm-wave transmission. The resulting response will depend on the relative significance of both superfluid and quasiparticle contribution. A more quantitative analysis will be given in section 7.4.

Relaxation Processes and Relaxation Times

In order to obtain a better understanding of the time scales involved, it is essential to imagine the nature of the processes involved in quasiparticle relaxation. The main scattering processes in conjunction with the recombination process have been represented in fig. 7.4 by their corresponding Feynman diagrams. As was shown in fig. 7.1, the thermalization process (B+C) occurs within approximately 1 ns. This involves all of the scattering processes given in fig. 7.1, including both *elastic* and *inelastic* scattering.

Relaxation times obtained in earlier experiments, both equilibrium and non-equilibrium-like, span a rather large time domain. From microwave cavity perturbation experiments, Bonn and co-workers [5] estimated the scattering time to be around 10^{-12} to 10^{-13} s,

quasiparticle - quasiparticle
scattering

quasiparticle - impurity
scattering

quasiparticle - phonon
scattering
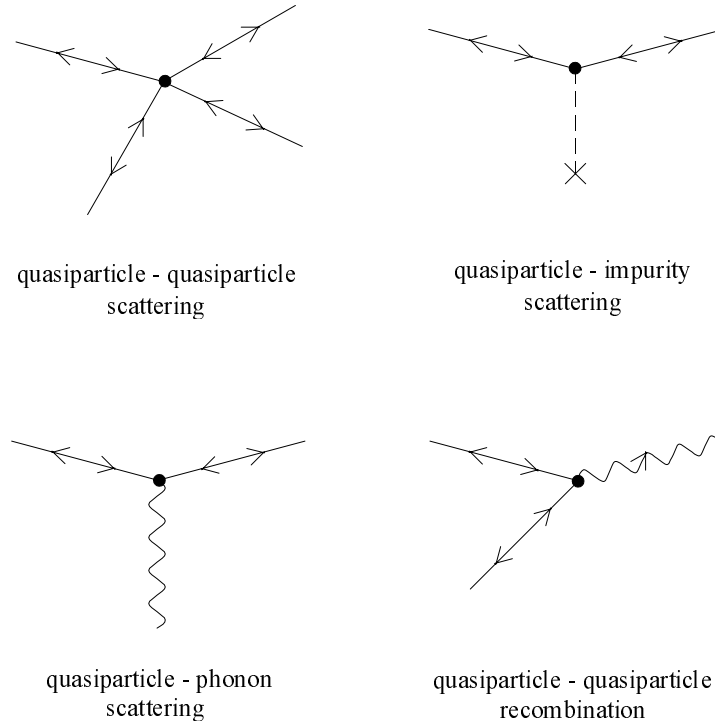
quasiparticle - quasiparticle
recombination

Figure 7.4: *Main scattering processes taking care of the thermalization of the excess quasi-particles depicted by their corresponding Feynman diagram. Also indicated is the recombination process.*

where they used the two-fluid model to obtain the absolute magnitude. In addition, data obtained by FIR-spectroscopy and dc-resistivity [19, 20], and results presented in chapter 6 of this thesis yield comparable scattering times. In all of these experiments however, one measures a combination of all relaxation processes, including elastic and inelastic scattering and the recombination process. In contrast, Doettinger *et al.* reported the scattering time to be strongly temperature dependent and rather long, up to a value of 10^{-8} s at 40 K [21]. In this experiment, they measured the critical vortex velocity which is predicted to be inversely proportional to the inelastic scattering time by Larkin and Ovchinnikov [22]. The physical reason for the close correlation is that inelastic scattering tends to move the quasiparticles within the vortex back to their equilibrium distribution, and therefore a vortex can reach a higher velocity before going through a transition. Since *elastic* scattering makes no contribution to the relaxation, one expects to measure a longer scattering time. This argument may explain the apparent discrepancy between their results and the microwave data. This also implies that it is natural to expect the pure recombination term to be on an even longer time scale than the one measured in the experiment of Doettinger *et al.*, since in this case neither elastic nor inelastic processes contribute.

In the PIAMA experiments the time resolution is around or slightly better than 1 μs. However, cascading and thermalization processes occur on a much faster time scale. Combining the information given above with the picture described in fig. 7.3, we can conclude that PIAMA is mainly sensitive to the *number* of quasiparticles. Therefore, since scattering merely changes the energy and not the density of quasiparticles, we measure only the recombination contribution.

Quasiparticle Relaxation in a d-wave Superconductor

A large variety of pump-probe and photoconductivity experiments have been performed in an attempt to determine the quasiparticle relaxation time [15–18, 23–27]. In all cases known to us, a high energy laser (> 1eV) has been utilized to create the excited state. Most workers found two contributions to the response, one having a fast and one having a relatively slow relaxation time. The fast contribution ranges from a few ps [17, 27] to several hundreds of ps [15, 24] and is usually attributed to non-equilibrium or non-bolometric effects.

This term covers many different phenomena such as a hot electron effect [27, 28] and a rapid change of the kinetic inductance [15,23]. In our case the temporal resolution ($\sim 1\mu$s) is insufficient to measure such responses. The second, slower response ranges from several ns [16] up to values in the μs-regime [24, 26, 29] and is usually attributed to bolometric effects. However, alternative explanations have also been given for the long-lived component such as photoinduced localized states [26] or the photofluxonic effect [30]. In the latter case a vortex-antivortex pair is created using a photon.

It is essential to realize that in contrast to all the above presented photoconductivity and pump-probe experiments, in our case the "pump" energy is relatively low, within the FIR-range. The reason why this is important

Figure 7.5: *Representation of an energy gap having a $d_{x^2-y^2}$ symmetry, showing the nodes at ($\pm\pi/2$, $\pm\pi/2$).*

can be understood pictorially using fig. 7.5, where the d-wave gap has been drawn in k-space. The functional form of a d-wave gap symmetry can be described by

$$\Delta(\mathbf{k}) = \Delta_{max}[\cos(k_x\,a) - \cos(k_y\,a)] \tag{7.3}$$

where Δ_{max} is the maximum gap, which is estimated experimentally to be around 200-250 cm^{-1} [31]. This means that the phonon energy provided by FELIX is comparable to or even smaller than $2\Delta_{max}$, thereby putting the quasiparticles into preferred excited states. The time constant of thermalization has been estimated to be around 1 ns [15], and hence
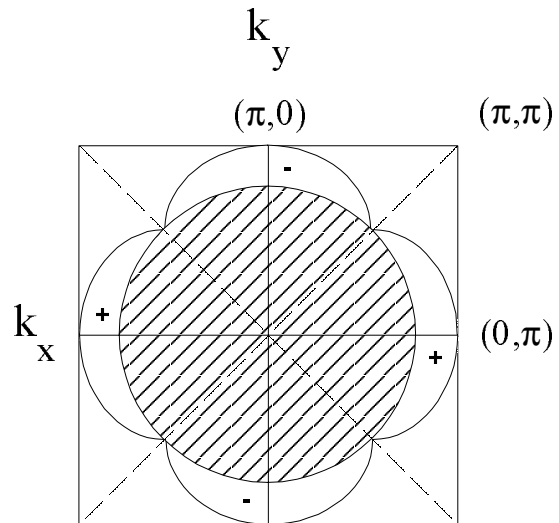
it is natural to assume that the quasiparticles will thermalize before they recombine, i.e. decay towards the nodes, according to the Fermi-Dirac distribution:

$$f_k(E, T, n) \;=\; \frac{1}{1 + e^{[E - \mu_{qp}]/k_B T}} \tag{7.4}$$

where E is the quasiparticle energy, μ_{qp} is the quasiparticle chemical potential and T is their equilibrium temperature. However, in the case of a d-wave symmetry, this implies that the quasiparticles end up in a well defined state having a momentum k close to $(\pm\pi/2, \pm\pi/2)$. This has been demonstrated more clearly in fig. 7.6, where the quasiparticle dispersion has been depicted for cuts along two different directions in k-space. The left panels show the
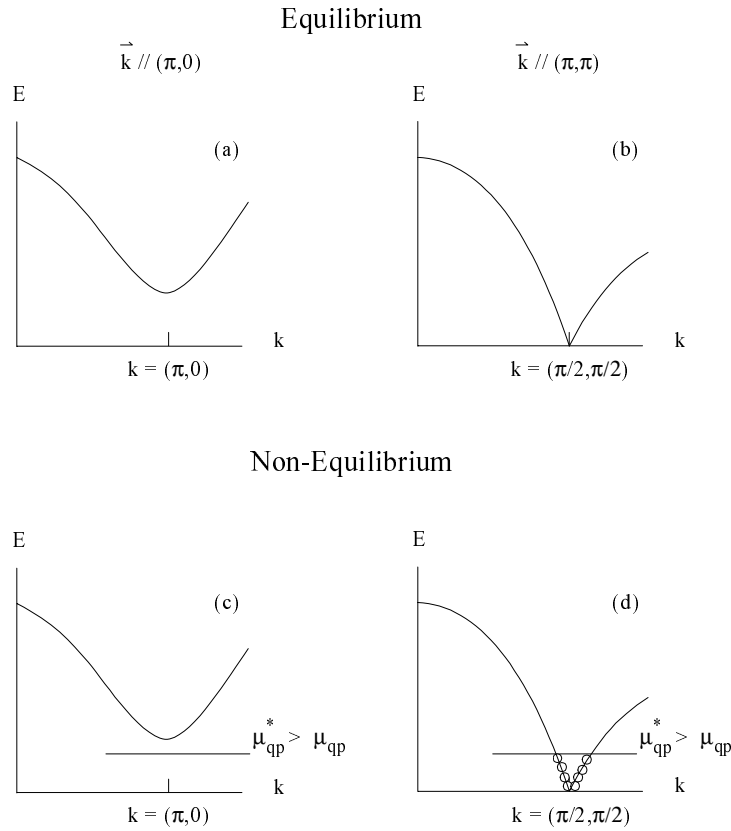
Figure 7.6: *Quasiparticle dispersion, showing the influence of the modified quasiparticle chemical potential μ_{qp}^*. The upper panels show the equilibrium response, whereas the lower panels depict the non-equilibrium case. In both cases the left panel is a cut taken along the $(\pi, 0)$ direction, while the right panel is a cut taken along the (π, π) direction.*

cut taken along the $(\pi,0)$ direction, reaching the largest value for the gap, Δ_{max}. The right panels show the cut taken along the (π, π) direction, i.e. in the direction of the nodes. As

before we can make a distinction between the two possible cases, the equilibrium response (upper two panels) and the non-equilibrium response (lower two panels). In the upper case the quasiparticle chemical potential is in equilibrium with its environment, and hence the Cooper pair and quasiparticle distribution functions attain their usual values, as if the sample resides at an elevated temperature. In contrast, in the lower panel the system temperature is in equilibrium, while μ_{qp} has been shifted. This clearly demonstrates that in the non-equilibrium case the probability for quasiparticles to be situated in the proximity of the nodes is much higher than the probability for other positions in k-space.

Realizing furthermore that in order to recombine, two quasiparticles have to fulfill kinematic quantum restrictions in order to conserve both energy and momentum, it is reasonable to expect that for carriers residing near the nodes, recombination is exceedingly difficult. This implies that in case of a d-wave symmetry the recombination time can be enhanced by orders of magnitude. A more quantitative analysis together with the precise formulation of the kinetic equations will be given in section 7.4.

7.3   NbN

In order to test the new technique of Photo Induced Activation of Mm-wave Absorption (PIAMA), we began by measuring a conventional superconductor. We used a NbN film with a thickness of 55 nm deposited on a 490 μm thick MgO substrate. The same film was studied in chapter 6 using mm-wave transmission measurements.

During all measurements a spurious oscillation, something in addition to the FIR induced changes, was observed. This oscillation was caused by cross talk between the laser electronics and our system, as could be checked by blocking the FELIX-beam with the free electron laser on. The oscillation was very reproducible and therefore we were able to eliminate its contribution by measuring with and without the FIR-radiation present on the sample. An example of two typical data sets, and the corrected transient is shown in fig. 7.7. The curves have been given an arbitrary vertical offset for the sake of clarity. We clearly see the oscillation in the data both with and without FELIX incident on the sample. After subtracting the reference signal, the photo induced change in transmission (PIT-signal) shows a smooth decay. The same correction procedure has been performed on all data presented below. In addition to the oscillation, all the data presented here have been corrected for the transfer function of the differentiating circuit connected to the diode detector, having a time constant of 45 μs. This was done by convoluting the measured responses with the exponential response function of the measurement circuit.

In fig. 7.8 we show the photo induced transmission (PIT-signal) for the NbN film measured at five different temperatures (4, 10, 12, 16 and 18 K from top to bottom). The pump frequency is 666 cm^{-1}, while the probe frequency is 150 GHz (5 cm^{-1}). The macropulse power was 16.0 mJ/pulse. The curves have been given an arbitrary vertical offset. Using the absolute unperturbed transmission in combination with the absolute value of the diode output, we can estimate the *change* in transmission coefficient from the measured voltages. We observe a positive change in the transmission coefficient due to the
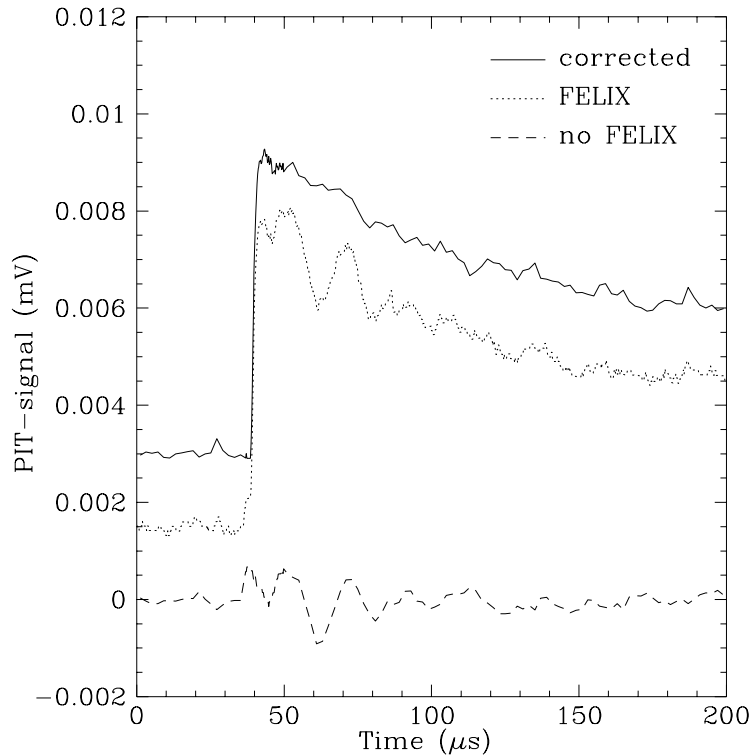
Figure 7.7: *Photo induced transmission shown both before (dotted line) and after (solid line) correcting for the spurious oscillation present in the transient. Also shown is the reference curve measured without the FELIX-beam incident on the sample (dashed line). The curves have been given an arbitrary vertical offset.*

presence of the FIR-radiation at all temperatures, up to T_c (17 K). This by itself is not sufficient information to conclude whether the response is bolometric or non-bolometric. However, we will argue below that, combining all the available information, we can conclude that in this case the superconductor remains in an equilibrium state, and the photo induced changes are due to a bolometric effect.

Evidence for the Bolometric Nature of the Response

When the signals are plotted on a logarithmic scale, as is done in the inset for the 4 and 16 K data, we see that the transmission decays exponentially, having a very slow relaxation time of the order of 100-200 μs. The exponential behavior and the long time constants are characteristic of a bolometric response, and are indicative of the photo induced transmission being due to an effective heating of the sample by the FIR-pulse. Upon lowering the temperature, two competing effects determine the thermal time constant of the system, since both the heat capacity and the thermal conductivity will be reduced. In fig. 7.9
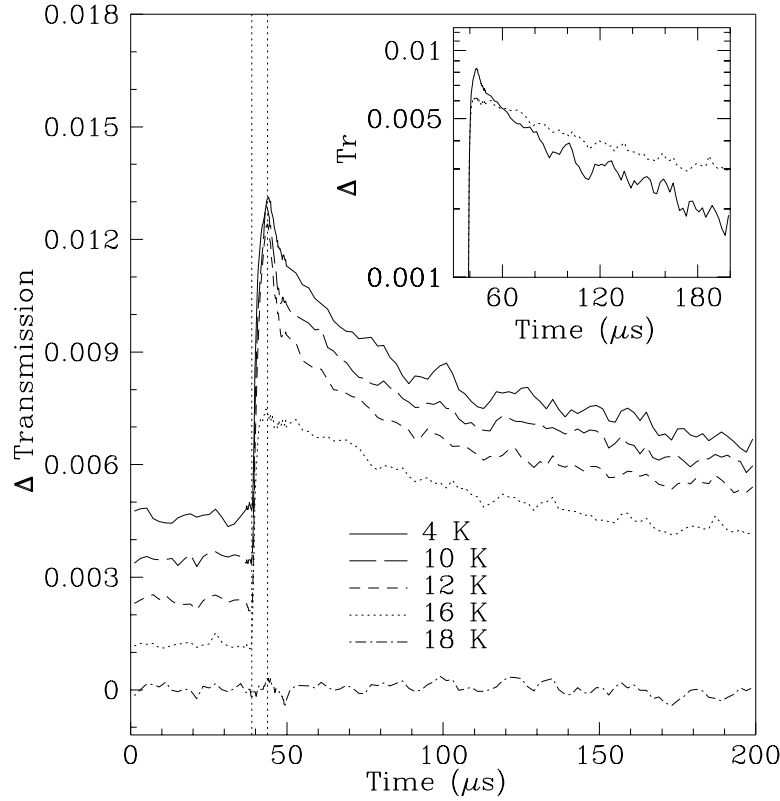
Figure 7.8: *Photo induced transmission for NbN on MgO at 4 K (solid), 10 K (dashed), 12 K (short dash), 16 K (dotted) and 18 K (dash-dotted). The curves have been given an arbitrary vertical offset. Inset: Δ Transmission plotted on a logarithmic scale at 4 and 16 K.*

the relaxation time is plotted as a function of temperature, again at a pump frequency of 666 cm^{-1} and a mm-wave frequency of 150 GHz. From the fact that the decay time is considerably faster at lower temperatures we conclude that in this particular case the heat capacity is reduced more severely.

In the upper panel of fig. 7.10 the maximum change in transmission, ΔTr, has been plotted as a function of temperature for the same frequencies as used above. In the lower panel, on the same temperature scale, the *unperturbed* transmission at 140 GHz through the same NbN film has been depicted. As was explained in chapter 6, the transmission at 150 GHz will be quantitatively slightly different due to interference effects, but the qualitative behavior, essential for the argument below, will be same.

Using the temperature dependence of the specific heat and the absorbed power, we can estimate the induced temperature rise, ΔT. We assume that the temperature rise will be homogeneous within the entire sample, hence ΔT can be calculated by $P/((C_p + C_e)V_f + C_s V_s)$. The specific heat of the MgO substrate, C$_s$, has been obtained by extrapolating
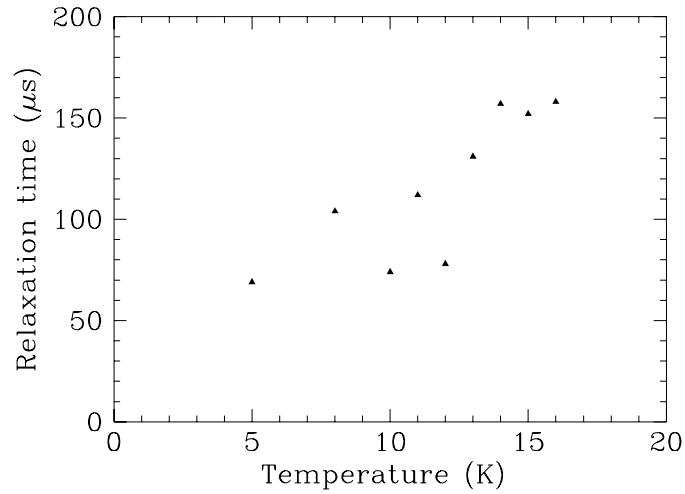
Figure 7.9: *Relaxation time of the photo induced transmission as a function of temperature, at $\nu_{fir} = 666\,cm^{-1}$ and $\nu_{mm} = 150\,GHz$.*
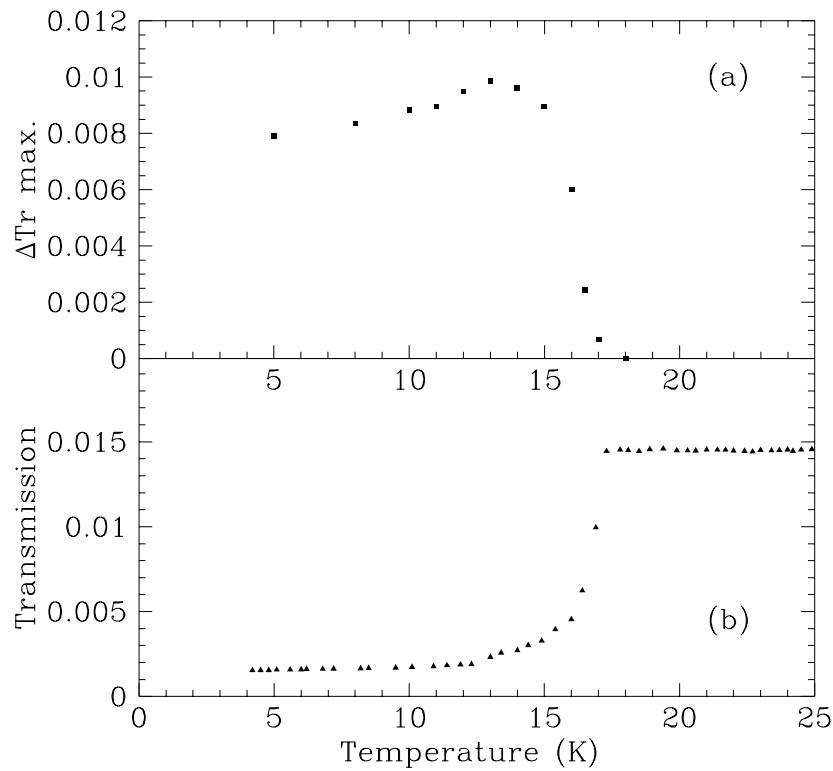

Figure 7.10: *a: Temperature dependence of the peak amplitude of the photo induced transmission at $\nu_{fir} = 666\,cm^{-1}$ and $\nu_{mm} = 150$ GHz. b: Temperature dependence of the unperturbed transmission at $\nu_{mm} = 140$ GHz.*

experimental data from ref. [32] to low temperatures. Since there are no experimental data of the phonon specific heat for NbN known to us, this quantity has been calculated using the Debye temperature ($\Theta_D \sim 250K$) [33]. This yields $C_p = (12\pi^4/5)nk_B(T/\Theta_D)^3 = 5.0 \times 10^{-3}$ Jcm^{-3}K^{-1} where we used $n = 4.8 \times 10^{22}$ cm^{-3}, the atom density of NbN. The electronic specific heat is 1.5×10^{-3} Jcm^{-3}K^{-1}, where both values were calculated at 8 K. In order to calculate the temperature dependence we used a T^3 dependence for C_p and $e^{-\Delta/kT}$ for C_e. We estimate the actual power absorbed within the sample to be $0.7 \times 0.7 \times 0.35 \times 0.5 \times 16 \times 10^{-3} = 1.37 \times 10^{-3}J$. In this case 0.7 is the transmissivity of one KRS-5 window, 0.35 is the absorptivity of the sample, 0.5 is the loss due to the nonzero angle of incidence, elongating the spot at the sample position, and 16 mJ is the power of a single macropulse, measured just before the cryostat. This yields ΔT of approximately 9.4 K starting at 4 K, while ΔT is gradually reduced to approximately 3 K at 15 K. In table 7.2 we compare the calculated temperature changes with the measured ones, while also the specific heat values are given for both substrate and film. Furthermore, the volume of the film was 55×10^{-7} cm^3 and the substrate contained 7.5×10^{-3} moles of LaAlO$_3$. The comparison demonstrates the fair agreement supporting the bolometric nature of the changes. The measured changes have been determined by combining the maximum change in the PIT-signal and the unperturbed transmission. The agreement is quite good, even

T (K)	ΔT_{th} (K)	ΔT_{exp} (K)	C$_{film}$ (mJ/cm^3 K)	C$_s$ (mJ/mole K)
4	9.4	12.5	1.2	4.9
8	6.8	8.8	6.5	13.1
10	5.4	6.9	17.1	21.8
11	4.8	5.9	26.3	26.6
12	4.3	4.9	38.5	31.8
13	3.8	> 4	54.0	38.6
14	3.4	> 3	73.0	45.6
15	2.9	> 2	97.7	53.2
16	2.6	> 1	121.9	62.1

Table 7.2: *Comparison of the theoretical and experimental temperature changes for NbN.*

though the model to estimate ΔT is rather crude. The remaining discrepancy is most probably caused by these simple assumptions. The strongly temperature dependent specific heat therefore provides a natural explanation for the fact that the peak amplitude is reduced less severely at low temperatures than one would expect if ΔT were assumed to be equal at 5 and 15 K.

This scenario explains furthermore the apparent correlation between the induced signal and the superconducting state. Since the temperature dependence of the transmissivity is rather small in the normal state due to the nearly constant conductivity, the PIT-signal vanishes above T$_c$. The PIT-signal is therefore not directly related to the presence of the

superconducting condensate, but to the *rate* at which the transmission changes.

Similar results as presented above were obtained at other pump frequencies. This is to be expected since the superconducting energy gap (2Δ) for NbN is approximately 50 cm^{-1}. Hence the frequency of FELIX is much larger than 2Δ. This inhibits a spectroscopic study of the energy gap in this material using FELIX.

7.4   DyBa$_2$Cu$_3$O$_{7-\delta}$

7.4.1   Results

In contrast to conventional superconductors, for high temperature superconductors the energy gap (or the maximum energy gap, Δ_{max}, in case of a d-wave superconductor) is of the order of several hundreds of wavenumbers, as are other relevant energy scales, such as phonon frequencies. This energy coincides nicely with the energy scale that can be covered using FELIX, allowing us to study the quasiparticle dynamics both as a function of frequency and temperature.

Temperature Dependence

In fig. 7.11 the unperturbed mm-wave transmission through a DyBa$_2$Cu$_3$O$_{7-\delta}$ film of 20 nm thickness, deposited on a 520 μm thick LaAlO$_3$ substrate is depicted for two frequencies, 120 and 150 GHz. The transmission at these frequencies is rather different, mainly due to interference effects within the film-substrate system. This has been explained in more detail in chapter 6. For the analysis below, the most significant property of the transmission coefficient is its *monotonic* temperature dependence over the entire range, at *all* frequencies. Focusing the attention on the 150 GHz curve, since we used this frequency in all PIAMA experiments, we see a nearly temperature independent transmission at higher temperatures, showing no evident drop at T$_c$ ($\sim$ 88 K). Only at lower temperatures the transmission is reduced more strongly, due to the enhanced significance of the superfluid fraction (see chapter 6).

In fig. 7.12 the photo induced transmission (PIT-signal, i.e. ΔTr) of the same film is shown for temperatures ranging from 5 to 70 K. The pump frequency is 800 cm^{-1}, while the probe frequency is 150 GHz. The curves have been corrected for long term instabilities in the incident power. The exact correction procedure will be explained in detail later in this section. We see that for temperatures lower than 40 K, the FIR-radiation *enhances* the transmissivity of the thin film. However, around 40 K the situation changes and the FIR pulse starts to *reduce* transmission instead. Moreover, exactly at 40 K the enhancement and the reduction of the PIT-signal are present simultaneously. Having the additional knowledge of the ordinary, *monotonic* behavior seen in the temperature dependence of the unperturbed mm-wave transmission we reason that a simple heating of the sample can never account for such a crossover. Furthermore, we see that the photo induced signal persists at 65 K, although it has a reduced amplitude. At this temperature however, the unperturbed transmission is already nearly temperature independent. This provides

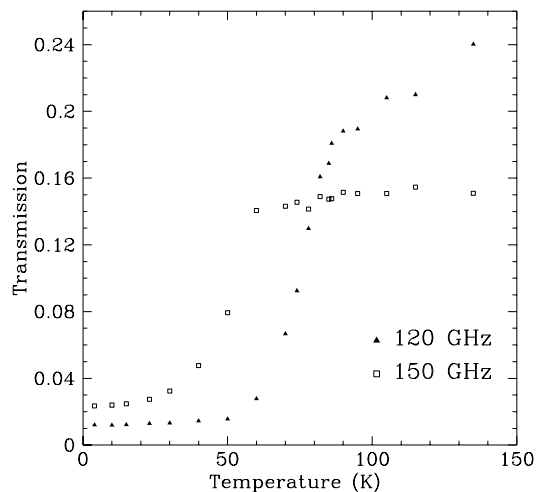Figure 7.11: *Unperturbed transmission through a $DyBa_2Cu_3O_{7-\delta}$ film on $LaAlO_3$, film thickness 20 nm, at ν=120 GHz (solid triangles) and 150 GHz (open squares).*
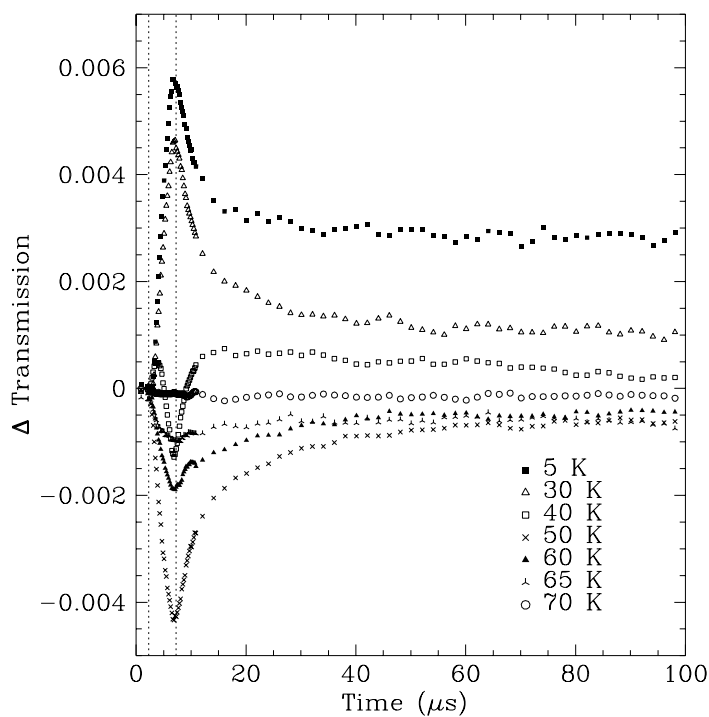

Figure 7.12: *Photo Induced Transmission for $DyBa_2Cu_3O_{7-\delta}$ on $LaAlO_3$, film thickness 20 nm, shown for several temperatures. The FIR-pulse enhances transmission at low temperatures, while it reduces it at temperatures higher than 40 K.*

additional evidence that the response cannot be due to an ordinary heating effect, since a purely bolometric signal would vanish. Around 70 K the PIT-signal drops below our detection limit, which inhibits us to draw definite conclusions about its evolution toward T_c. Also above T_c no change in transmission was observed.

In order to explain the observed behavior we return to the argument given in section 7.2. We now concentrate on the lower two panels of fig. 7.3 on page 120, in which the non-equilibrium response is sketched. Assuming that we can describe the superconducting state using a two-fluid model, we are sensitive to the contribution of both the superfluid and the normal fluid fraction. The former is represented by the δ-function at zero-frequency, responsible for the superconductivity. The spectral weight within the δ-function is determined by the number of Cooper pairs present, and will be reduced during the presence of a FIR-pulse. This will result in a less effective screening of the incident field and therefore the transmission will be enhanced temporarily, as can be seen in eq. (7.2). The quasiparticle contribution is represented by the Drude-peak in σ_1, centered around zero-frequency and having a finite width ($\gamma_{qp} = 1/\tau_{qp}$). During the pair-breaking process, the spectral weight within this peak is strongly enhanced. Under the assumption that the electron temperature relaxes within a few nanoseconds, which is considerably faster than our time resolution, on our time scale the shifted chemical potential will be the dominant effect. We can therefore regard the scattering rate γ_{qp} to retain its equilibrium value. Hence, at lower frequencies, the conductivity due to the quasiparticle peak will be considerably higher than in the initial state, thereby temporarily enhancing the *absorption* within the superconductor. When this contribution is more dominant than the reduced Cooper pair density the transmission will be reduced.

The explicit behavior, such as the temperature at which the crossover from a positive to a negative PIT-signal occurs, will strongly depend on several parameters. First, the precise values and temperature dependencies of the intrinsic sample properties such as σ_1 and the penetration depth λ will be vital. In principle, since σ_1 has a non-monotonic behavior as a function of temperature, for cuprates a situation can occur in which even the unperturbed response will be non-monotonic. In this particular situation however, we know that this is not the case and an alternative explanation for the sign change in the PIT-signal is needed. A second parameter becomes clear from fig. 7.3: if we would tune the probe frequency to a considerably higher value, the increase in absorption due to the enhanced conductivity will be less pronounced and the negative PIT-signal will subdue.

Frequency Dependence

The dependence of the PIT-signal on the frequency of the pump at T = 40 K is shown in fig. 7.13. In order to correct the spectra for the altered output power of FELIX at different frequencies within one scan of the undulator magnetic field, we also studied the power dependence of the PIT-signal. The change in power is within 10 % for most of the band that can be reached in this way, except for the frequencies at both sides of the band where the output power diminishes rapidly. The results at 5 K using a pump frequency of 750 cm^{-1} are shown in fig. 7.14. The power indicated in the figure is measured for a single

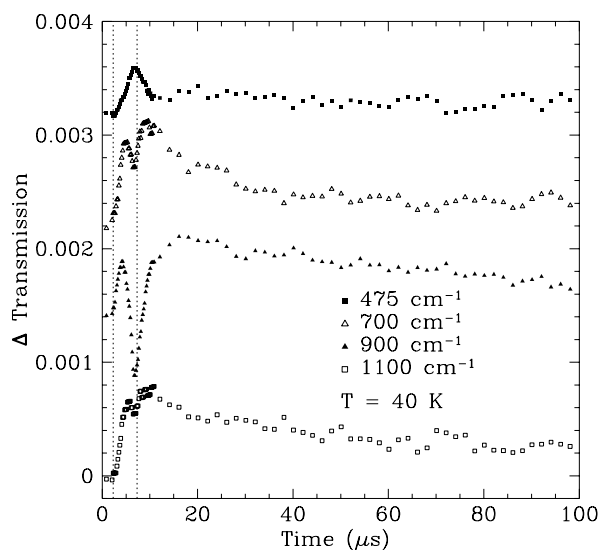Figure 7.13: *Photo Induced Transmission shown for several different frequencies at $T = 40$ K. At this temperature for some of the frequencies both the positive and the negative influence of the FIR-pulse are clearly visible. The curves have been given an arbitrary vertical offset.*
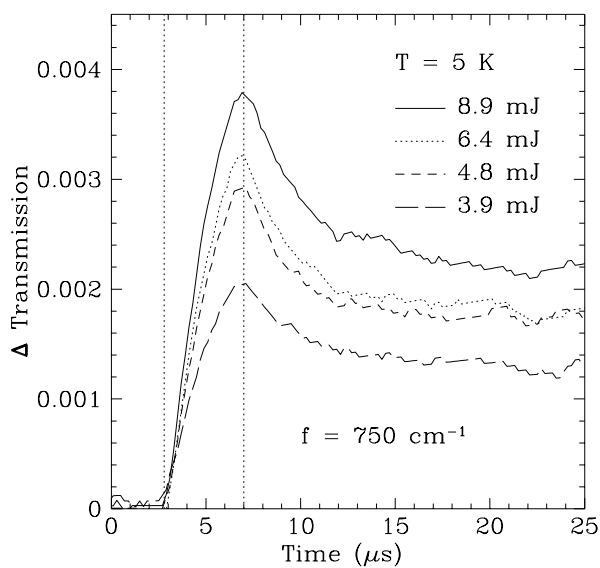

Figure 7.14: *Power dependence of the peak amplitude of the PIT-signal. The pump frequency is 750 cm^{-1}, while the temperature is 5 K.*

macropulse just before the cryostat. The normalized peak amplitudes, where we divided the maximum induced change in transmission by the input power, are 0.40, 0.48, 0.53 and 0.48 for the highest to the lowest incident power respectively. Therefore we assume that we are approximately within the linear regime and we can take the changing laser fluence into account by dividing the spectra by the measured pulse power. This was done after normalizing the pulse powers to the highest value within the band. Such a procedure conserves the observed absolute change in transmission, enabling us to obtain a direct correlation between ΔTr and ΔT. The power measured outside the cryostat is reduced by a factor of 0.5 in passing two KRS-5 windows, but since this factor is nearly frequency independent, as can be seen in fig. 4.6 on page 75, this does not enter the frequency or the temperature dependence. Moreover, from fig. 7.14 we conclude that within the power range used during the PIAMA experiments, the changes are not affected by saturation effects. In addition we conclude from the linear power dependence of the signal that one photon absorption processes govern the response.

In order to acquire the complete frequency dependence ranging from 320 - 1400 cm^{-1}, we needed two different settings for the accelerator voltage. The reproducibility of the observed changes has been carefully checked by examining the overlapping parts of the frequency ranges.

The experimental behavior presented above is indicative of reaching a critical quasiparticle density, both as a function of temperature and frequency. Returning to the equations (7.1) and (7.2) we can estimate the relative significance of both quasiparticle and Cooper pair density at all temperatures. Therefore we need to calculate the change in transmission coefficient due to changes in both σ_1 and λ. Equation (7.2) yields:

$$\Delta Tr = (Tr)^2 \left[-2\pi(1 + p^2 + \frac{4\pi d\sigma_1}{c})\frac{d\sigma_1}{p^2 c}\left(\frac{\Delta\sigma_1}{\sigma_1}\right) + \frac{d^2 c^2}{2p^2\omega^2\lambda^4}\left(\frac{\Delta(\lambda^2)}{\lambda^2}\right) \right] \tag{7.5}$$

We can thus calculate the relative importance of both terms by determining α and β where we used:

$$\Delta Tr = -\alpha\left(\frac{\Delta\sigma_1}{\sigma_1}\right) + \beta\left(\frac{\Delta(\lambda^2)}{\lambda^2}\right) \tag{7.6}$$

Using the information we obtained from the unperturbed transmission experiments shown in fig. 6.15 and 6.16 we obtain the results given in table 7.3. For those values that are not available, we used extrapolations similar to the experimental results reported in references [34] and [35] for σ_1 and λ, respectively. Although β is larger than α up to about 60 K, it is clear that the σ_1-term attains considerable weight upon raising the temperature. Whereas it has no significant influence on ΔTr at 5 K, at higher temperatures it becomes much more dominant.

To establish the idea of reaching a critical quasiparticle density experimentally, we have studied the coexistence of the positive and negative PIT-signal at 40 K in more detail. The photo induced transmission has been plotted along with the FELIX pulse in fig. 7.15 for three different pulse lengths, using an arbitrary vertical offset for the sake of clarity. It is

T (K)	α ($\times 10^{-3}$)	β ($\times 10^{-3}$)
5	2.9	45.6
15	4.3	43.3
30	13.2	39.6
40	18.1	34.2
50	24.5	36.7
60	35.8	17.8
70	37.6	4.1

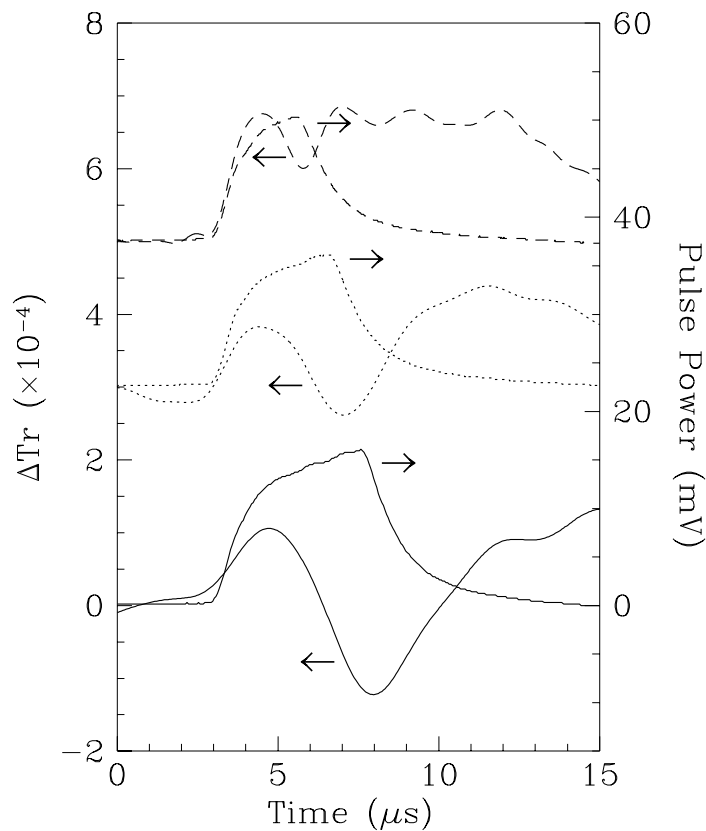Table 7.3: *Prefactors α and β from eq. (7.6) demonstrating the significance of σ_1 and λ.*

Figure 7.15: *left axis: Photo induced transmission at 40 K using ν_{fir} = $630\,cm^{-1}$. The curves are showing the response to FIR-pulses (right axis) of three different lengths, 4 μs (dashed), 5 μs (dotted) and 6 μs (solid). The curves have been given an arbitrary vertical offset for the sake of clarity.*

evident that the start of the dip in transmission is independent of the pulse length. At this point the number of excited quasiparticles is sufficiently large, thereby causing the absorption due to the enhanced conductivity to govern the PIT-signal. It is also clear that the onset of the second increase in transmission corresponds to the termination of the pulse. The PIT-signal returns to a positive value due to the remaining bolometric change in the sample state.

Comparison to Absorptivity

The changes in transmission as a function of pump frequency show a rather non-monotonic behavior and have been summarized in fig. 7.16 for several temperatures ranging from 5 to 60 K. Plotted are the absolute peak heights obtained after the correction for the changes in incident power. Here we divided the measured peak voltage by the pulse power directly. This procedure hence yields both positive and negative values. In order to include the 40 K data, the positive (A) and the negative contribution (B) have been determined separately, while the *total* induced change (A-B) is included in fig. 7.16. Remarkable is that the positive contribution, A, remains nearly constant, as soon as the negative contribution sets in.

In fig. 7.16, we have also plotted the frequency dependence of the absorptivity, A, within the *film*. This has been calculated using the Fresnel equations for a stratified system and the case of an anisotropic film.

$$A \;=\; 1 - |r_{lr}|^2 \;-\; |t_{lr}|^2 \tag{7.7}$$

The complex reflection and transmission coefficients r_{lr} and t_{lr} have been determined in section 3.2.2. In the calculation the angle of incidence was equal to 45° and a mixture of 50 % s- and 50 % p-polarized light was assumed, identical to the experimental situation. For the film properties we used the dielectric function at 10 K of $YBa_2Cu_3O_{7-\delta}$ obtained from reflectivity measurements [36,37]. Both the ab-plane and the c-axis dielectric function have been drawn in fig. 7.17 in the left and right panel respectively. The dielectric function of the substrate can be described by a sum of Lorentz phonon oscillators:

$$\epsilon \;=\; \epsilon_\infty \;+\; \sum_{j=1}^{N} \frac{S_j \omega_j^2}{\omega_j^2 - \omega\left(\omega + i\gamma_j\right)} \tag{7.8}$$

We utilized the experimental phonon parameters presented in ref. [38]. These parameters have been summarized in table 7.4. The substrate phonons modify the absorptivity

$\epsilon_\infty = 4.0$			
phonon	ω_j (cm^{-1})	γ_j (cm^{-1})	S$_j$
#1	185	3.1	15.0
#2	427	4.2	4.2
#3	498	6.5	0.014
#4	594	7	0.005
#5	651	15	0.27
#6	674	49	0.014

Table 7.4: *Substrate parameters used for the calculation of the absorptivity of the $DyBa_2Cu_3O_{7-\delta}$ film on a $LaAlO_3$ substrate.*
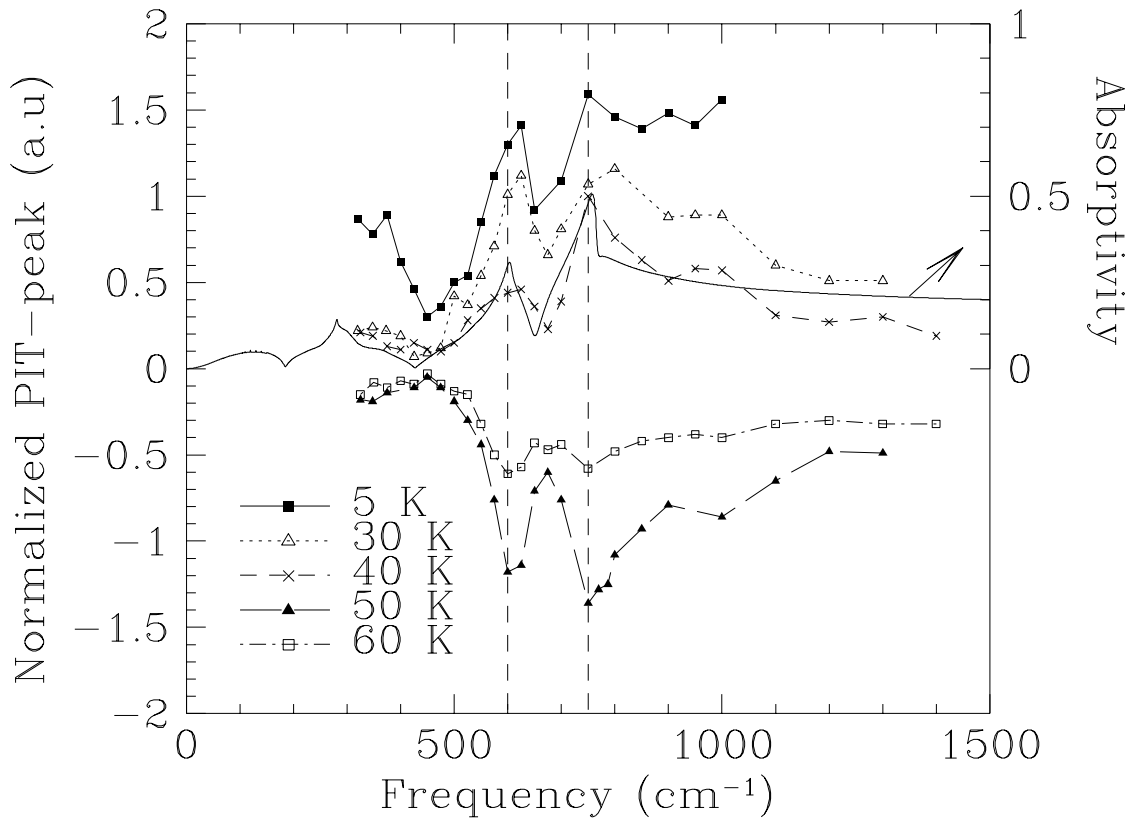
Figure 7.16: *Normalized peak intensity as a function of frequency, shown for several different temperatures, ranging from 5 to 60 K. At 40 K the sum of the positive and the negative peak has been plotted. The absorptivity within the film is shown as the solid line.*

Figure 7.17: *Left: ab-plane dielectric function as a function of frequency for $YBa_2Cu_3O_{7-\delta}$. Right: c-axis dielectric function. In both cases ϵ' is indicated by the solid line and ϵ'' by the dotted line.*

within the film rather severely. Instead of having a smooth behavior expected in case of a single Drude contribution, peaks appear at frequencies corresponding to the *longitudinal* substrate phonon 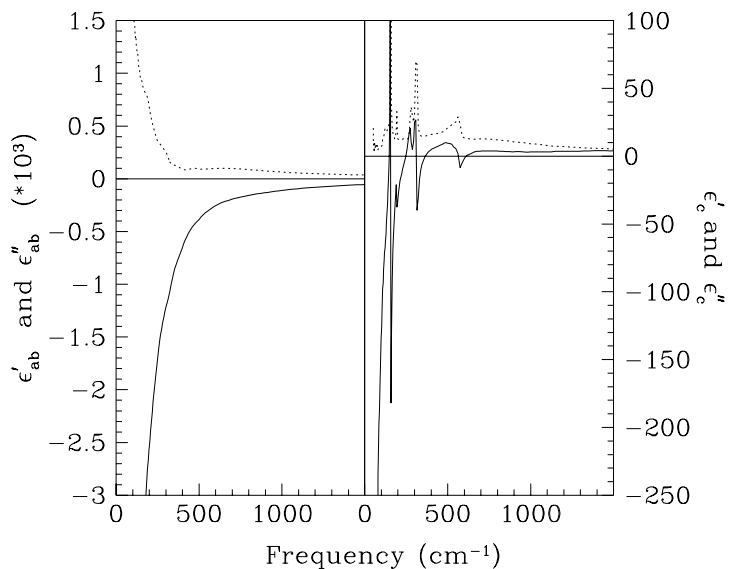frequencies. Due to the high reflectivity of the substrate within its Reststrahlenbands the matching between the film and the substrate changes, giving rise to an enhanced absorption within the film, a phenomenon known as the Berreman effect [39]. Remarkable is that the c-axis phonons of the film, clearly visible in ϵ_c' and ϵ_c'', play no role in determining the absorptivity within the film. It has been shown under similar conditions in chapter 5 of this thesis and in ref. [40] that c-axis phonons appear in the reflectivity and they can therefore be expected in the absorptivity as well. The absence of these structures is most likely caused by the small film thickness.

We notice that the overall structure of the absorptivity within the film corresponds very well to the normalized peak amplitude of the PIAMA response. This demonstrates that it is possible to measure the absorption within the film very sensitively in this way.

It is important to note that the absorptivity of the substrate itself is in fact maximal *at* the transverse phonon frequencies, corresponding to the minima in the absorptivity within the film, presented in fig 7.16 as the solid line. This establishes that the observed features are not due to substrate heating, since the PIT-peak amplitude has minima at the transverse substrate phonon frequencies, in contrast to the substrate absorptivity.

7.4.2 Discussion of the Relaxation Times and the Kinetic Restrictions related to the d-wave Symmetry

Finally, in this section we will discuss the observed relaxation times in the context of bolometric and non-bolometric contributions. Furthermore a theoretical treatment will be presented, using the point of view of the dispersion relations as well as an approach using a set of coupled kinetic equations.

Time Constants

In fig. 7.18 a typical pulse shape, which has been renormalized for comparison, is shown in conjunction with the 30 K transient. We see clearly that the relaxation process does not follow the pulse at *any* time, implying that the measured relaxation time is indeed generic for the relaxation process within the sample, and *not* limited by the pulse shape. An exception to this observation might be the dip measured at 40 K. In the inset of fig. 7.18 a comparison between the same pulse and the 40 K transient is made. We see that the slope of the relaxation follows the pulse, indicating that the actual process might be even faster. Knowing from the negative response at higher temperatures that the induced changes in transmission are not due to a heating effect, and realizing that the relaxation time is not limited by experimental factors, we need to explain the unusually long life time of the non-equilibrium state.

In order to obtain a quantitative idea on the measured time constants, we fitted the
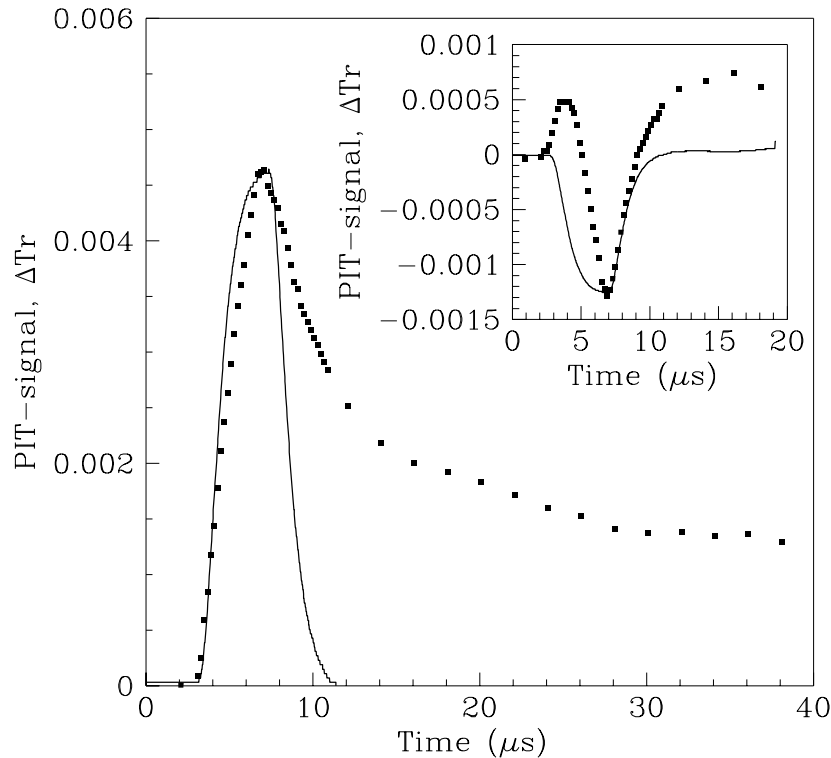
Figure 7.18: *Comparison of the incident pulse shape (solid line) and the observed changes in transmission at 30 K. The same comparison at 40 K is shown in the inset. In both cases the pulse has been renormalized for comparison.*

transients using a linear combination of two exponentially decaying signals.

$$\Delta Tr = I_1 e^{-t/\tau_1} + I_2 e^{-t/\tau_2} \tag{7.9}$$

The results of these fits can be seen in fig. 7.19. For the fit we have concentrated on the initial decay, up to 45 μs, because the slope of the decay on longer time scales is very sensitive to the magnitude of the differentiating time constant, used to correct the transients for the influence of the diode detector. The relaxation times obtained in this fashion, are given in table 7.5 and plotted in fig. 7.20 as a function of temperature. The second component was only needed at the lower temperatures (5, 30 and 40 K), to obtain a reasonable fit. The time constants of the second contribution have been indicated as τ_2 in table 7.5. We attribute the second, positive component to an appreciable bolometric response, only present at lower temperatures due to the much smaller specific heat. Disregarding the fast response for this moment, we estimate that the PIT-signal would be due to a temperature rise of approximately 13 K by comparing the measured amplitude with the unperturbed transmission curve. Similar arguments lead to an experimental temperature rise of approximately 1.5 K for the 30 K response and 0.2 K for the 40
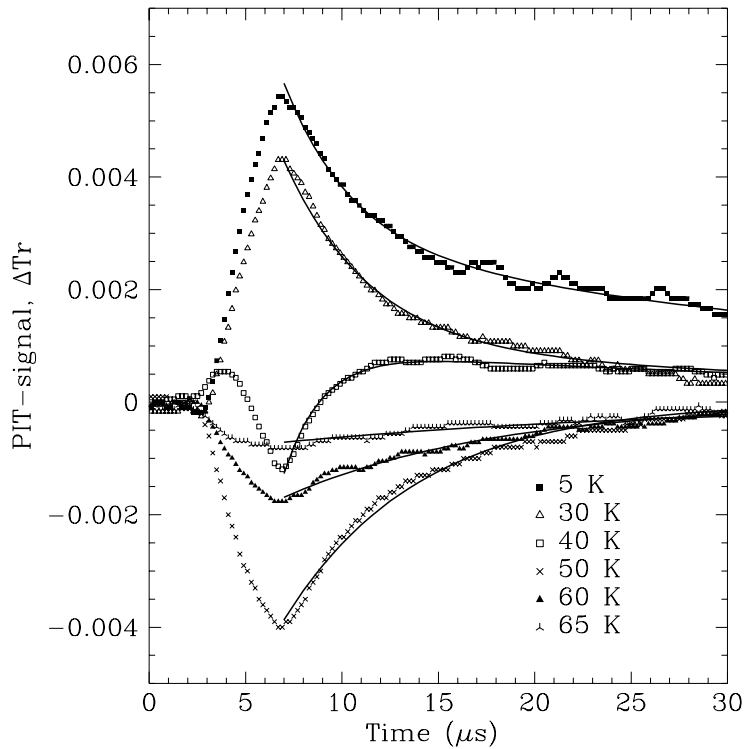
Figure 7.19: *Photo induced transmission plotted for several temperatures, together with an exponential fit. The pump frequency is 800 cm^{-1} and the probe frequency is 150 GHz.*
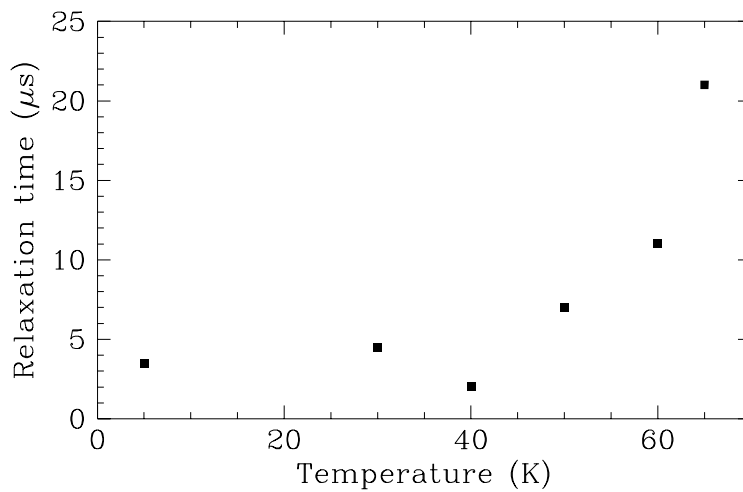

Figure 7.20: *Temperature dependence of the relaxation time obtained from the exponential fit of the PIAMA-transients at 800 cm^{-1}.*

T (K)	τ_1 (μs)	τ_2 (μs)
5	3.5	> 45
30	4.5	> 45
40	2.0 (-)	> 45 (+)
50	7	-
60	11	-
65	21	-

Table 7.5: *Relaxation times obtained from the exponential fit of the PIAMA-transients at 800 cm^{-1}.*

K transient. At 40 K we used the height of the positive peak directly after the fast non-bolometric dip. At temperatures higher than 40 K an experimental value for the temperature rise can not be obtained, since a resulting change in transmission will never be negative. Moreover, at temperatures higher than 60 K the unperturbed transmission is nearly temperature independent, implying that any observed change in transmission can not be bolometric.

In a similar fashion as for the NbN-film, we can *calculate* the expected temperature rise of the DyBa$_2$Cu$_3$O$_{7-\delta}$ film using the absorbed power and the specific heat of the entire system. The maximum pulse power during the temperature scan was 11.6 mJ/pulse, yielding $0.7 \times 0.7 \times 0.5 \times 0.25 \times 11.6 \times 10^{-3} = 0.71 \times 10^{-3}$ J as the power which is actually absorbed within the film. For the specific heat of the film we used the experimental values presented in ref. [41]. The specific heat of the substrate has been extrapolated using a T^3 dependence, starting from C$_s$ = 30.2 J/mole K at 77 K and taking 720 K as the Debye temperature [42]. As the molar densities we used 2.5×10^{-7} and 1.45×10^{-3} for the film and the substrate respectively. These numbers immediately show that the influence of the film can be neglected in the calculation of ΔT. The results are summarized in table 7.6 in conjunction with the estimated experimental values. We find that the size of ΔT_{exp} for

T (K)	ΔT_{th} (K)	ΔT_{exp} (K)	C$_{film}$ (J/mole K)	C$_{sub}$ (J/mole K)
5	8.7	13	0.01	8.1×10^{-3}
30	0.34	1.5	1.9	1.8
40	0.18	0.2	3.7	4.2

Table 7.6: *Comparison of the experimental and theoretical temperature changes for DyBa$_2$Cu$_3$O$_{7-\delta}$.*

the slow contribution can be described fairly well in this way. Therefore we conclude that at higher temperatures, due to the much larger specific heat of both film and substrate, the incident power barely changes the sample temperature.

Dispersion Relations

In this section we want to make the inhibition of the recombination process somewhat more physically transparent by looking at the dispersion relations of the gap function, the quasiparticles and the phonons emitted during recombination.

Our main interest will be the transition probability from a state involving two quasiparticles and N Cooper pairs into a state with N+1 Cooper pairs and an emitted phonon, i.e. the recombination process:

$$\gamma_R \;=\; |<(N_{q\lambda}+1)|\gamma_{k\uparrow}\gamma_{k'\downarrow}a_{q\lambda}^{\dagger}|N_{q\lambda}, k\uparrow k'\downarrow>|^2 \tag{7.10}$$

where $\gamma_k, \gamma_{k'}$ are the quasiparticle operators, written in terms of the electron operators C and $C^{\dagger}$ [43]:

$$\begin{aligned}
\gamma_{ek0}^{\dagger} &= u_k C_{k\uparrow}^{\dagger} \,-\, v_k S_k^{\dagger} C_{-k\downarrow} \\
\gamma_{ek1}^{\dagger} &= u_k C_{-k\downarrow}^{\dagger} \,+\, v_k S_k^{\dagger} C_{k\uparrow} \\
\gamma_{hk}^{\dagger} &= S_k \gamma_{ek}^{\dagger}
\end{aligned} \tag{7.11}$$

Here S $(^{\dagger})$ is the *pair* annihilation (creation) operator and u_k and v_k are the well-known BCS coherence factors

$$\begin{aligned}
v_k^2 &= \frac{1}{2}\left[1 - \frac{\xi_k}{E_k}\right] \\
u_k^2 &= 1 - v_k^2
\end{aligned} \tag{7.12}$$

where ξ_k is the quasiparticle energy at momentum k and $E_k \;=\; (\Delta_k^2 + \xi_k^2)^{1/2}$.

In the quasiparticle recombination process the coherence factor for pair creation is

$$(v_k u_{k'} \,+\, u_k v_{k'})^2 \;\approx\; \frac{1}{2}\left(1 + \frac{\Delta_k^2}{E_k E_k}\right) \tag{7.13}$$

assuming that $|\vec{k}| \approx |\vec{k'}|$. Substituting eq. (7.13) into (7.10) finally yields

$$\tau_R \;=\; \frac{1}{\gamma_R} \;\sim\; \frac{1}{\Delta_k} \tag{7.14}$$

This result can be understood intuitively, knowing that the transition probability is in fact a measure of the overlap of the quasiparticle wavefunction and the superconducting energy gap function. Therefore, in case of a smaller gap the transition probability will be smaller and hence the quasiparticle lifetime will be longer. In fact, precisely at the nodes the energy gap vanishes, and consequently the recombination time would be infinite. In reality there are always physical processes breaking the symmetry yielding a finite τ_R, such as scattering processes involving two phonons. However, since these are second order processes having a lower probability, τ_R is likely to be long.

Obviously, both momentum and energy conservation laws will have to be satisfied in the recombination process, yielding:

$$\begin{aligned}
\vec{k} + \vec{k'} &= \vec{q} \\
E_k + E_{k'} &= v_s|q|
\end{aligned} \tag{7.15}$$

where v_s is the sound velocity within the material. By plotting the dispersion relation for quasiparticles close to the nodes, it becomes clear that, for a gap dispersion which is steep compared to the linear phonon dispersion, satisfying both conservation laws simultaneously is problematic. A qualitative sketch can be seen in fig. 7.21. In order to improve the lucidity of the figure, we have used a few transformations that do not affect the validity of the argument. First we only consider two quasiparticles close to opposite nodes, such as for instance close to $(\pi/2, \pi/2)$ and $(-\pi/2, -\pi/2)$. (see fig. 7.5 for the d-wave gap symmetry). Since, in the other cases, the difference in momentum taken up by the phonon will be very large, and consequently the emitted phonon energy will be rather large, the transition becomes less probable. In order to move the cones on top of each other, we have plotted δk and δq according to

$$\vec{k} = \left(\frac{\pi}{2}, \frac{\pi}{2}\right) + \delta k, \quad \vec{q} = \left(\frac{\pi}{2}, \frac{\pi}{2}\right) + \delta q \tag{7.16}$$

where $\vec{k}$ is the momentum vector parallel and $\vec{q}$ the momentum vector perpendicular to the Fermi surface. Furthermore, for the case of the node at $(-\pi/2, -\pi/2)$, we define the difference in momentum as $-\delta k$ and the energy as $-E_{\delta k}$. This transformation rotates this cone by 180° around the $\vec{k}_z$-axis and by 180° around the $\vec{q}$-axis. The conservation laws given in eq. (7.15), under these transformations become:

$$\begin{aligned}
\delta\vec{k} - \delta\vec{k'} &= \vec{q} \\
E_{\delta k} - E_{\delta k'} &= v_s|q|
\end{aligned} \tag{7.17}$$

The functional form of the dispersion of the quasiparticles, plotted in fig. 7.21, is given by

$$E_{\delta k} = \hbar\sqrt{(\delta k)^2 \left(\frac{\partial \Delta_k}{\partial k}\right)^2 + (\delta q)^2 v_F^2} \tag{7.18}$$

where the functional form of the energy gap, Δ_k, has been given in eq. (7.3) and v_F is the Fermi velocity. For a quasiparticle in a state $(\delta k, 0)$, indicated by the large dot, there is a range of possible quasiparticle states in the lower cone available for recombination, indicated by the ellipse. However, if the phonon dispersion, represented by the dashed lines, is considerably shallower than the slope of the gap around the nodes, there will be no phonon states available to consume the remaining momentum and energy.

Assuming that the only effect of an increased sample temperature is a reduction of the size of the maximum gap at $(\pi, 0)$, the slope of the quasiparticle dispersion will decrease at higher temperatures. Hence, around a certain temperature the dispersion of the gap and the phonons will be comparable, yielding a minimum in the relaxation time. In contrast, upon approaching T_c from below, $\Delta_{max} \rightarrow 0$, implying, using eq. (7.14), that τ_R will be consequently enhanced.
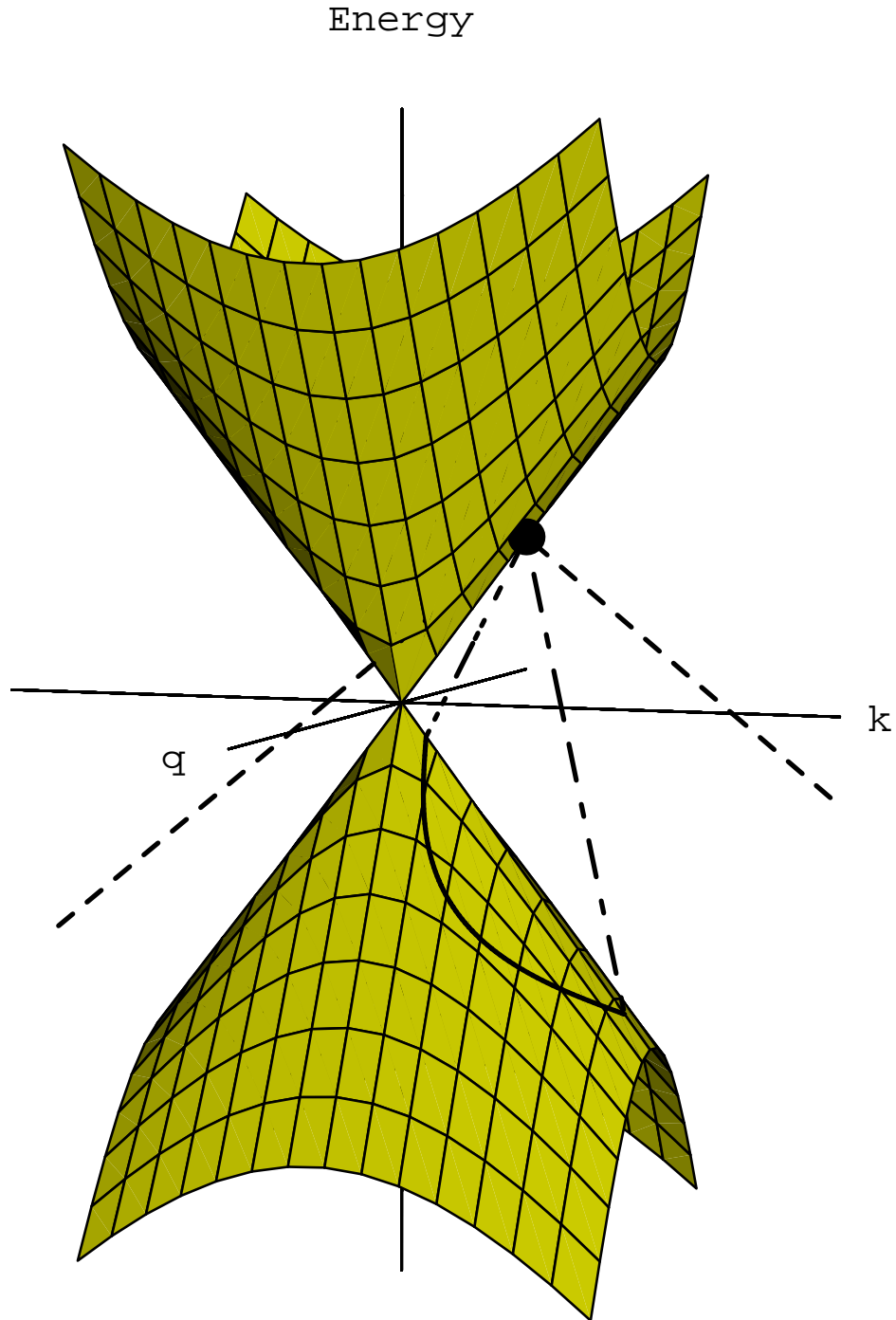
Figure 7.21: *Qualitative sketch of the quasiparticle dispersion in opposite nodes in conjunction with a linear phonon dispersion (dashed line). This clearly demonstrates the occurrence of a bottleneck if the former is too steep.*

Kinetic Equation Approach

We used a kinetic equation approach to describe a superconductor in a non-equilibrium state, in order to obtain a *quantitative* idea about the relaxation and recombination processes. The kinetic approach was first introduced by Bardeen *et al.* [44] to study the thermal conductivity of a superconductor and was later adapted to the strong coupling case by Ambegeokar and Tewordt [45] and Prange and Kadanoff [46, 47]. Considering the superconductor as a combined system involving three different components (quasiparticles, phonons and Cooper pairs) leads to the construction of set of coupled equations describing their respective distribution functions. This approach is equivalent to the more rigorous Green's function approach [48], while the resulting equations are rather transparent while still incorporating the essential physics within the problem.

We begin by constructing the coupled equations describing the non-equilibrium distribution functions of the quasiparticles, f(E_k), and the phonons, n(Ω_q).

$$\begin{aligned}
\frac{df(E_k)}{dt} &= I_{qp}(E_k) + \frac{\partial f(E_k)}{\partial t} \\
\frac{dn(\Omega_q)}{dt} &= I_{ph}(\Omega_q) + \frac{\partial n(\Omega_q)}{\partial t}
\end{aligned} \tag{7.19}$$

Here I_{qp}(E_k) and I_{ph}(Ω_q) are energy spectra of the quasiparticle and phonon injection rate, respectively. We will restrict our discussion here to the case where a pulsed optical source is used to create the non-equilibrium state. Therefore I_{ph}(Ω_q) is always equal to zero, whereas I_{qp}(E_k) is nonzero only during the pulse. Immediately after the pulse we study a *free* quasiparticle relaxation. The second terms in both expressions describes the changes in time of the respective distribution functions.

Concentrating first on this part of the coupled equations for the case of the quasiparticles, the resulting contribution will be a combination of many scattering processes. The main processes have been treated in the beginning of this chapter, and it is important to realize once again that elastic and inelastic scattering and recombination all contribute in the relaxation process. In our case, we have established that, due to the temporal resolution, the transients are not affected by the fastest processes, such as quasiparticle-quasiparticle scattering and the cascading process in which quasiparticles decay via additional pair-breaking. Moreover, the quasiparticle-impurity scattering only contributes to the collision rate if the process is inelastic. The contribution of the elastic processes vanishes due to the cancellation of coherence factors. Such processes however, still play a role in the relaxation process for an anisotropic superconductor because, although leaving the energy unaffected, they can still modify the momenta of the quasiparticles.

Our main aim will be to calculate the quasiparticle-phonon scattering. Not only we can estimate the phonon scattering time and its temperature dependence, but most importantly we can make a direct comparison between the *scattering* and the *recombination* process due to their similarity. The Hamiltonian for the electron-phonon interaction can be written

as [49]:

$$H_{e-ph} \; = \; \sum_{p\sigma,q\lambda} g_{q\lambda} C^{\dagger}_{p+q,\sigma} C_{p\sigma} \left(a_{q\lambda} \; + \; a^{\dagger}_{-q\lambda} \right) \tag{7.20}$$

where $C(^{\dagger})$ is the electron annihilation (creation) operator and p, σ and q, λ are the momenta and spin quantum numbers for electrons and phonons respectively, while $g_{q\lambda}$ is the electron-phonon coupling parameter. In order to rewrite this in a useful form for quasiparticles, we use the Bogoliubov transformation to the quasiparticle operators. Substituting eq. (7.11) into (7.20) yields:

$$\begin{aligned}
H_{e-ph} = \sum_{p,q,\lambda} g_{q\lambda} &\left\{ L(p+q,p) \left[\gamma^{\dagger}_{e(p+q)0} \gamma_{ep0} \; + \; \gamma^{\dagger}_{ep1} \gamma_{e(p+q)1} \right] \right. \\
&\left. + M(p+q,p) \left[\gamma_{e(p+q)0} \gamma_{hp1} \; - \; \gamma_{ep0} \gamma_{h(p+q)1} \right] \right\} \left(a_{q\lambda} \; + \; a^{\dagger}_{-q\lambda} \right)
\end{aligned} \tag{7.21}$$

where the coherence factors are now given by:

$$\begin{aligned}
L(p',p) &\equiv u_{p'} u_p \; - \; v_{p'} v_p \; = \; \frac{1}{2} \left(1 \; - \; \frac{\Delta_p^2 - \xi_p \xi_{p'}}{E_p E_{p'}} \right) \\
M(p',p) &\equiv u_{p'} v_p \; + \; v_{p'} u_p \; = \; \frac{1}{2} \left(1 \; + \; \frac{\Delta_p^2 - \xi_p \xi_{p'}}{E_p E_{p'}} \right)
\end{aligned} \tag{7.22}$$

for scattering and pair creation or annihilation respectively. Furthermore, Δ_p is the superconducting energy gap, ξ_p is the quasiparticle excitation energy and $E_p \; = \; (\xi_p^2 \; + \; \Delta_p^2)^{1/2}$. Finally, using Fermi's golden rule for the transition rate, we can formulate the quasiparticle-phonon contribution to the kinetic equations.

$$\begin{aligned}
\frac{\partial f(\xi_p)}{\partial t} = \frac{2\pi}{\hbar} \sum_{q\lambda} &\left\{ |g_{q\lambda}|^2 \, L^2(p+q,p) \left[f(\xi_{p+q}) \left(1 - f(\xi_p) \right) \left(n(\Omega_{q\lambda}) + 1 \right) \right. \right. \\
&\left. - \, (1 - f(\xi_{p+q})) f(\xi_p) n(\Omega_{q\lambda}) \right] \delta(\Omega_{q\lambda} + E_p - E_{p+q}) \; - \; \left\{ p \leftrightarrow (p+q) \right\} \right\} \\
- \frac{2\pi}{\hbar} \sum_{q\lambda} &\left\{ |g_{q\lambda}|^2 \, M^2(p+q,q) \left[f(\xi_p) f(\xi_{p+q}) (n(\Omega_{q\lambda}) + 1) \right. \right. \\
&\left. - \, (1 - f(\xi_p))(1 - f(\xi_{p+q})) n(\Omega_{q\lambda}) \right] \delta(E_p + E_{p+q} - \Omega_{q\lambda}) \right\}
\end{aligned} \tag{7.23}$$

Here $f(\xi_i)$, for i = p,p+q, and $n(\Omega_{q\lambda})$ are the occupation numbers for the quasiparticles and the phonons respectively. Using an identical argumentation as above one can write down a similar term for the phonon kinetic equation. We will restrict the discussion to the most essential part, the quasiparticle non-equilibrium distribution.

We can distinguish four different terms in eq. (7.23), which are easily recognizable from their occupation numbers. The first two terms are the quasiparticle-phonon scattering contributions, where the first involves phonon emission, and the second phonon absorption. The last two terms describe the quasiparticle recombination contribution, involving the emission of a phonon, and the phonon induced pair breaking, respectively.

Since all terms, in fact, describe the rate at which the densities grow or diminish, (7.23) still needs to be divided by the density $f(\xi_p)$, in order to obtain the actual scattering rates for a quasiparticle having momentum p. This yields, for instance, for the recombination term:

$$,_R \;=\; \frac{1}{\tau_R} \;=\; \frac{2\pi}{\hbar}\sum_{q,\lambda}|g_{q\lambda}|^2\,M^2(p+q,p)\,f(\xi_{p+q})\,(n(\Omega_{q\lambda})+1)\delta(E_p+E_{p+q}-\Omega_{q\lambda}) \tag{7.24}$$

where the other terms are calculated in a similar fashion.

For $f(\xi_i)$ we used the Fermi-Dirac distribution

$$f_k(\xi_i,T,n) \;=\; \frac{1}{1+e^{[\xi_i-\mu]/k_BT}} \tag{7.25}$$

while for the phonon density of states the Boltzmann distribution was used

$$n(\Omega_{q\lambda}) \;=\; \frac{1}{e^{\hbar\omega_q/k_BT}-1} \tag{7.26}$$

Using the information given above and the temperature dependence of the energy gap, and therefore the temperature dependence of the occupation numbers L(p',p) and M(p',p), we are able to calculate all four contributions individually at all temperatures, besides the unknown electron-phonon coupling parameter $g_{q\lambda}$. However, $g_{q\lambda}$ appears in all contributions, allowing a direct comparison, even though the absolute magnitudes of the scattering rates are unknown. In fig. 7.22 the scattering time, τ_{in}, resulting from a sum of both scattering processes (phonon absorption and emission) is depicted in conjunction with the recombination time, τ_R. The time constants were calculated using a Monte-Carlo approach, averaging over the entire k-space, where the fact that quasiparticles are mainly situated in the nodes is included via the Fermi-Dirac distribution. The most striking observation is the enhancement of more than two orders of magnitude of τ_R compared to τ_{in}. In the calculation we assumed a perfect two-dimensional system, allowing no dispersion in the c-axis direction. A finite hopping in the c-axis direction might tend to bring both curves closer to one another.

Moving our focus to the temperature dependence of both quantities, we see that the scattering time is reduced upon increasing the temperature, as expected. The temperature dependence of τ_{in} is not as strong as the one observed experimentally by Doettinger *et al.* [21], which can be attributed to the presence of additional inelastic scattering contributions such as quasiparticle-quasiparticle scattering in the latter case. These contributions cannot be compared directly to the recombination process due to the different prefactors. However, we know from the rapid reduction of the scattering rate just below T_c [4,50] that quasiparticle-quasiparticle scattering is in fact very important in these materials. Inclusion of this process in the calculation of τ_{in} will tend to move both curves in fig. 7.22 further apart, while the temperature dependence of τ_{in} will be enhanced.

The recombination time, τ_R, is fairly temperature independent at low temperatures and has a minimum around $0.8\times T_c$ due to an optimal matching of the phonon and the
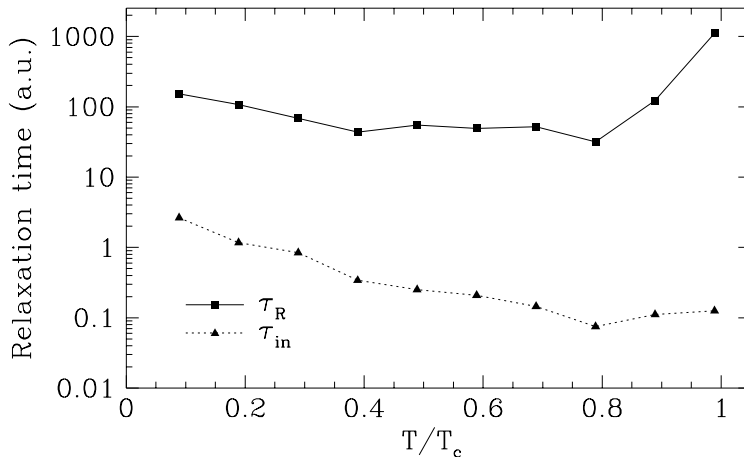
Figure 7.22: *Temperature dependence of the quasiparticle-phonon scattering time (τ_{in}, tri-angles) and the quasiparticle recombination time (τ_R, squares).*

quasiparticle dispersion. At the higher temperatures τ_R shows a tendency to increase due to the reduced size of the gap. The experimental recombination times plotted in fig. 7.20 show a temperature dependence in accordance with the one observed in fig. 7.22, including the weak temperature dependence at low temperatures, while showing an increase upon approaching T_c. The minimum, predicted by the calculations, seems to be present as well, explaining the fact that the 40 K transient is the only one presumably limited by the pulse shape.

Noteworthy is furthermore, that Frenkel and co-workers [16] observed a similar temperature dependence, but explained the enhancement of τ by a factor of 4 by a growing contribution of the bolometric component within the total response.

7.5   Conclusions

We have observed non-equilibrium superconductivity within $DyBa_2Cu_3O_{7-\delta}$ using Photo Induced Activation of Mm-wave Absorption (PIAMA), whereas we observed a purely bolometric response for NbN. For NbN the calculated temperature changes agree fairly well with the experimentally observed changes in transmission. The bolometric explanation is supported furthermore by the long time scales (100-200 μs) and the reduced amplitude at low temperatures.

The unique tunability of the free electron laser (FELIX) allowed us to study PIAMA as a function of frequency for energies both below and above the relevant energy scales in $DyBa_2Cu_3O_{7-\delta}$. The frequency dependence resembles the calculated absorptivity spectrum for a thin film deposited on a $LaAlO_3$ substrate. Since the PIAMA response is minimum at frequencies corresponding to the Reststrahlen absorptions in the substrate, we conclude

that substrate heating is unimportant.

As a function of temperature the induced changes cross over from being positive at T < 40 K, indicating an enhanced transmission, to being negative at T > 40 K, due to a reduced transmission. The temperature dependence is indicative of reaching a critical quasiparticle density at which the photo induced signal starts to be dominated by the dissipative part of ϵ, rather than the inductive part. This behavior can be explained qualitatively by assuming a two-fluid description in the superconducting state. The reduced Cooper pair density is causing an enhancement of transmissivity, while an enhanced absorption due to the influence of the non-equilibrium quasiparticles reduces the transmission at higher temperatures. It is impossible to explain the sign change by a purely bolometric effect, since the unperturbed mm-wave transmission shows a monotonic behavior as a function of temperature. Moreover, heating of the sample has been calculated to become rather insignificant at higher temperatures, which is supported by the presence of a second, slow ($> 45\mu$s) contribution. This contribution is only present at T $\leq$ 40 K and shows an enhanced transmission for all cases.

The observed relaxation time of the non-equilibrium state is unusually long, 2 to 20 μs. We propose that, due to the unique use of a FIR laser in this experiment in combination with a high T$_c$ superconductor, the quasiparticles, after thermalization, end up in the nodes of the d-wave energy gap. Having a well defined momentum state, recombination of quasiparticles is inhibited due to kinetic considerations. This picture is supported by calculations comparing the quasiparticle-phonon scattering time and the recombination time directly, showing an enhancement of about two orders of magnitude of the latter. The predicted temperature dependence of τ_R, being nearly constant at low temperatures while showing an enhancement at temperatures close to T$_c$, corresponds fairly well to the experimentally observed behavior.

References

[1]   for a review of the normal state properties in relation to the Fermi liquid approach see: K. Levin *et al.*, Physica C **175**, 449-522 (1991).

[2]   Basically the theoretical approaches can be subdivided into two streams. First the modified Fermi liquid theories such as the Marginal Fermi liquid theory (Varma *et al.*, PRL **63**, 1996 (1989)) and the Nearly Antiferromagnetic theory of Pines and co-workers (Monthoux *et al.*, PRL **69**, 961 (1992)) and Scalapino and co-workers (N. Bulut *et al.*, PRB **47**, 2742 (1993)). The second stream are the non-Fermi liquid approaches, such as the interlayer coupling model of Anderson and co-workers (S. Chakravarty *et al.*, Science **261**, 337 (1993)). See also chapter 2 of this thesis.

[3]   Martin C. Nuss, P. M. Mankiewich, M. L. O'Malley, E. H. Westerwick and Peter B. Littlewood, Phys. Rev. Lett. **66**, 3305 (1991).

[4]   D. A. Bonn, P. Dosanjh, R. Liang and W. N. Hardy, Phys. Rev. Lett. **68**, 2390 (1992).

[5]   D. A. Bonn, S. Kamal, Kuan Zhang, Ruixing Liang, D. J. Baar, E. Klein and W. N. Hardy, Phys. Rev. B **50**, 4051 (1994).

[6] O. Klein and G. Grüner, Comment on "Microwave Determination of the Electronic Scattering Time in YBa$_2$Cu$_3$O$_7$", Phys. Rev. Lett. **72**, 1390 (1994).

[7] P. L. Richards, J. Clarke, R. Leoni, Ph. Lerch, S. Verghese, M. R. Beasly, T. H. Geballe, R. H. Hammond, P. Rosenthal and S. R. Spielman, Appl. Phys. Lett. **54**, 283 (1989).

[8] R. S. Nebosis, R. Steinke, P. T. Lang, W. Schatz, M. A. Heusinger, K. F. Renk, G. N. Gol'tsman, B. S. Karasik, A. D. Semenov and E. M. Gershenzon, J. Appl. Phys. **72**, 5496 (1992).

[9] C. S. Owen and D. J. Scalapino, Phys. Rev. Lett. **28**, 1559 (1972).

[10] Jhy-Jiun Chang and D. J. Scalapino, Phys. Rev. B **9**, 4769 (1974).

[11] W. H. Parker, Phys. Rev. B **12**, 3667 (1975).

[12] L. R. Testardi, Phys. Rev. B **4**, 2189 (1971).

[13] A. Rothwarf, G. A. Sai-Halasz and D. N. Langenberg, Phys. Rev. Lett. **33**, 212 (1974).

[14] see for instance: G. M. Knippels, R. F. X. A. M. Mols, A. F. G. van der Meer, D. Oepts and P. W. van Amersfoort, Phys. Rev. Lett. **75**, 1755 (1995).

[15] N. Bluzer, Phys. Rev. B **44**, 10222 (1991).

[16] A. Frenkel, M. A. Saifa, T. Venkatesan, P. England, X. D. Wu and A. Inam, J. Appl. Phys. **67**, 3054 (1990).

[17] S. G. Han, Z. V. Vardenay, K. S. Wong, O. G. Symko and G. Koren, Phys. Rev. Lett. **67**, 3054 (1990).

[18] G. L. Eesley, J. Heremans, M. S. Meyer, G. L. Doll and S. H. Liou, Phys. Rev. Lett. **65**, 3445 (1990).

[19] F. Gao, J. W. Kruse, C. E. Platt, M. Feng and M. V. Klein, Appl. Phys. Lett. **63**, 2274 (1993).

[20] M. I. Flik, Z. M. Zhang, K. E. Goodson, M. P. Siegal and Julia M. Phillips, Phys. Rev. B **46**, 5606 (1992).

[21] S. G. Doettinger, R. P. Huebener, R. Gerdemann, A. Kühle, S. Anders, T. G. Träuble and J. C. Villégier, Phys. Rev. Lett. **73**, 1691 (1994).

[22] A. I. Larkin and Yu. N. Ovchinnikov, Zh. Exsp. Teor. Fiz. **68**, 1915 (1975)[Sov. Phys. JETP **41**, 960 (1976)].

[23] F. A. Hegmann, D. Jacobs-Perkins, C.-C. Wang, S. H. Moffat, R. A. Hughes, J. S. Preston, M. Currie, P. M. Fauchet and T. Y. Hsiang, Appl. Phys. Lett. **67**, 285 (1995).

[24] W. R. Donaldson, A. M. Kadin, P. H. Ballentine and R. Sobolewski, Appl. Phys. Lett. **54**, 2470 (1989).

[25] C. J. Stevens, D. Smith, C. Chen, J. F. Ryan, B. Podobnik, D. Mihailovic, G. A. Wagner, J. E. Evetts, Phys. Rev. Lett. **78**, 2212 (1997).

[26] C. J. Stevens, T. N. Thomas, S. Choudhury, J. F. Ryan, D. Mihailovic, L. Forro, G. A. Wagner and J. E. Evetts, SPIE **2696**, 313 (1996).

[27] M. Danerud, D. Winkler, M. Lindgren, M. Zorin, V. Trifonov, B. S. Karasik, G. N. Gol'tsman and E. M. Gershenzon, J. Appl. Phys. **76**, 1902 (1994).

[28] M. Zorin, M. Lindgren, M. Danerud, B. S. Karasik, D. Winkler, G. Gol'tsman and E. Gershenzon, J. Supercond. **8**, 11 (1993).

[29] H. S. Kwok, J. P. Zheng, Q. Y. Ying and R. Rao, Appl. Phys. Lett. **54**, 2473 (1989).

[30] A. M. Kadin, M. Leung and A. D. Smith, Phys. Rev. Lett. **65**, 3193 (1990).

[31] Matthias C. Schabel, C.-H. Park, A. Matsuura, Z.-X. Shen, D. A. Bonn, Ruixing Liang and W. N. Hardy, Phys. Rev. B. **55**, 2796 (1997).

[32] E. S. R. Gopal, *Specific Heats at Low Temperatures*, (Plenum, London, 1966).

[33] A. D. Semenov, R. S. Nebosis, Yu. P. Gousev, M. A. Heusinger and K. F. Renk, Phys. Rev. B **52**, 581 (1995).

[34] U. Dähne, Y. Goncharov, N. Klein, N. Tellmann, G. Kozlov and K. Urban, J. Supercond. **8**, 129 (1995).

[35] L. A. de Vaulchier, J. P. Vieren, Y. Guldner, N. Bontemps, R. Combescot, Y. Lemaitre and J. C. Mage, Europhys. Lett. **33** (2), 153 (1996).

[36] D. van der Marel, M. Bauer, E. H. Brandt, H.-U. Habermeier, D. Heitmann, W. König and A. Wittlin, Phys. Rev. B **43**, 8606 (1991).

[37] M. Bauer, Graduate Dissertation, University of Tübingen, 1990.

[38] Z. M. Zhang, B. I. Choi, M. I. Flik and A. C. Anderson, J. Opt. Soc. Am. B **11**, 2252 (1994).

[39] D. W. Berreman, Phys. Rev. **130**, 2193 (1963).

[40] J. H. Kim, B. J. Feenstra, H. S. Somal, D. van der Marel, Wen Y. Lee, A. M. Gerrits and A. Wittlin, Phys. Rev. B **49**, 13065 (1994).

[41] M. B. Maple, Y. Dalichaouch, J. M. Ferreira, R. R. Hake, B. W. Lee, J. J. Neumeier, M. S. Torikachvili, K. N. Yang, H. Zhou, R. P. Guertin and M. V. Kuric, Physica B **148**, 155 (1987).

[42] Peter C. Michael, John U. Trefny and Baki Yarar, J. Appl. Phys **72**, 107 (1992).

[43] M. Tinkham, *Introduction to Superconductivity*, (McGraw-Hill, New York, 1975 and Krieger, New York, 1980).

[44] J. Bardeen, G. Rickazen and L. Tewordt, Phys. Rev. **113**, 982 (1959).

[45] V. Ambegeokar and L. Tewordt, Phys. Rev. **34**, 805 (1964).

[46] R. E. Prange and L. P. Kadanoff, Phys. Rev. **34**, 566 (1964).

[47] for a review on the kinetic equation approach see: Jhy-Jiun Chang, Chapter 9 in *Nonequilibrium Superconductivity, Phonons and Kapitza Boundaries*, Kenneth E. Gray ed. (Plenum Press, New York, 1981).

[48] G. M. Eliashberg, Zh. Exsp. Teor. Fiz. **38**, 966 (1960) [Sov. Phys. JETP Lett. **11**, 696 (1960)].

[49] J. R. Schrieffer, *Theory of Superconductivity*, (Benjamin, New York, 1964).

[50] B. J. Feenstra, F. C. Klaassen, D. van der Marel, Z. H. Barber, R. Pérez Pinaya and M. Decroux, Physica C **278**, 213 (1997).